Multiple-Mode Orthogonal Frequency Division Multiplexing With Index Modulation

Miaowen Wen, *Member, IEEE*, Ertugrul Basar, *Senior Member, IEEE*,
Qiang Li, Beixiong Zheng, and Meng Zhang

***Abstract*— Orthogonal frequency division multiplexing with index modulation (OFDM-IM) performs transmission by considering two modes over OFDM subcarriers, which are the null and the conventional M-ary signal constellation. The spectral efficiency (SE) of the system, however, is limited, since the null mode itself does not carry any information and the number of subcarrier activation patterns increases combinatorially. In this paper, a novel IM scheme, called multiple-mode OFDM-IM (MM-OFDM-IM), is proposed for OFDM systems to improve the SE by conveying information through multiple distinguishable modes and their full permutations. A practical and efficient mode selection strategy, which is constrained on the phase shift keying/quadrature amplitude modulation constellations, is designed. Two efficient detectors that provide different tradeoffs between the error performance and detection complexity are also proposed. The principle of MM-OFDM-IM is further extended to the in-phase and quadrature components of OFDM signals, and the method of generating multiple modes from the M-ary pulse amplitude modulation constellation for this modified scheme is also introduced. Bit error rate (BER) analyses are provided for the proposed schemes. Monte Carlo simulations on BER corroborate the analyses and show that the proposed schemes appear as promising multi-carrier transmission alternatives by outperforming the existing OFDM-IM counterparts.**

***Index Terms*— OFDM, index modulation, in-phase/quadrature components, log-likelihood ratio (LLR), maximum-likelihood (ML), bit error rate (BER).**

I. Introduction

INDEX modulation modulation (IM) [1], [2], which utilizes the index(es) of the building blocks of the communications systems, such as antennas [3]–[5], subcarriers [6]–[9], spreading codes [10]–[12], and time slots [13], as an information carrying mechanism, is a novel digital modulation concept. Since the index(es) are embedded into the transmitted or received signals, which consume little or even no power, IM is capable of striking an attractive tradeoff between the spectral efficiency (SE) and energy efficiency (EE) of the system, making itself a competitive candidate for the fifth generation (5G) and beyond wireless communications systems [1], [2].

IM in the frequency domain is usually performed with the aid of either the frequency carriers or orthogonal frequency division multiplexing (OFDM) subcarriers. Frequency quadrature amplitude modulation (FQAM) is one of the well-known realizations of IM that modulate signals via frequency carriers [14]. In FQAM, frequency shift keying (FSK) and quadrature amplitude modulation (QAM) are combined to provide a desired tradeoff between the transmit power and the SE of the system. The most recent studies show that by employing FQAM in a downlink OFDM access system, the inter-cell interference is not Gaussian and the system capacity can be increased [15]. On the other hand, spatial modulation (SM), which is a pioneering IM technique in the space domain that investigated extensively in recent years [3]–[5], have motivated the researchers to consider the idea of using OFDM subcarriers for IM. The first attempt was the so-called subcarrier index modulation OFDM (SIM-OFDM) [6], in which each subcarrier is loaded by one IM bit and the subcarriers associated with the majority bit value are activated for data transmission. To avoid ambiguity, in SIM-OFDM, half of the available subcarriers transmit M-ary modulated symbols and the remaining active subcarriers are dedicated to control signaling. However, the erroneous detection of a subcarrier state will lead to the incorrect demodulation of subsequent subcarrier signals. To solve this error propagation problem, an enhanced SIM-OFDM (ESIM-OFDM) scheme was later proposed in [7]. Unlike SIM-OFDM, ESIM-OFDM uses one IM bit to control two adjacent subcarriers such that only one subcarrier is activated for each subcarrier pair. At the receiver, the subcarrier state can be easily determined by comparing its received signal power with that of its adjacent subcarrier. Unfortunately, the SE of ESIM-OFDM systems tends to be much smaller than that of classical OFDM systems for larger values of M since only one IM bit is available within each subcarrier group. This limitation was successfully relaxed in [8], where a flexible number of IM bits are involved in the process of information conveying and the term OFDM with index

Manuscript received January 10, 2017; revised April 12, 2017; accepted May 20, 2017. Date of publication May 31, 2017; date of current version September 14, 2017. This work was supported in part by the National Natural Science Foundation of China under Grants 61431005 and 61501190, in part by the Natural Science Foundation of Guangdong Province under Grant 2016A030308006, and in part by the open research fund of National Mobile Communications Research Laboratory, Southeast University under Grant 2017D08. The associate editor coordinating the review of this paper and approving it for publication was R. Dinis. *(Corresponding author: Miaowen Wen.)*

M. Wen is with the School of Electronic and Information Engineering, South China University of Technology, Guangzhou 510640, China, and also with the National Mobile Communications Research Laboratory, Southeast University, Nanjing 210096, China (e-mail: eemwwen@scut.edu.cn).

E. Basar is with the Faculty of Electrical and Electronics Engineering, Istanbul Technical University, Istanbul 34469, Turkey (e-mail: basarer@itu.edu.tr).

Q. Li and B. Zheng are with the School of Electronic and Information Engineering, South China University of Technology, Guangzhou 510640, China (e-mail: eeqiangli@mail.scut.edu.cn; zheng.bx@mail.scut.edu.cn).

M. Zhang is with the School of Electronics and Computer Science, Peking University, Beijing 100871, China (e-mail: mannyzhang@pku.edu.edu).

Color versions of one or more of the figures in this paper are available online at http://ieeexplore.ieee.org.

Digital Object Identifier 10.1109/TCOMM.2017.2710312

modulation (OFDM-IM) is coined. It is worth noting that a similar idea appeared earlier in 1999 [9]; however, the emergence of OFDM-IM has brought to the public an entirely new horizon from the IM concept.

In OFDM-IM, some of the available subcarriers are activated to transmit M-ary modulated symbols and the remaining subcarriers keep idle in each OFDM frame. The subcarrier activation pattern (SAP) is determined by an additional bit stream according to either the nature binary code [9], the combinatorial method [8], or the equiprobable subcarrier activation method [16]. The OFDM-IM signal can be detected efficiently by the log-likelihood ratio (LLR) based [8] and low-complexity maximum-likelihood (ML) [17] receivers, whose computational complexity is identical to that of the classical OFDM. Theoretical analyses in terms of uncoded bit error rate (BER) reveal that since the IM bits have a stronger protection than the ordinary modulation bits, OFDM-IM outperforms classical OFDM at the same SE [8]. This attractive advantage has motivated a great deal of follow-up research recently. Instead of localized subcarrier grouping, the interleaved subcarrier grouping is suggested for OFDM-IM to obtain frequency diversity in [18] and [19]. A tight upper bound on the BER of OFDM-IM in the presence of perfect and imperfect detection of SAPs is provided in [20]. The optimal subcarrier activation strategy in the sense of maximizing the achievable rate is designed for OFDM-IM in [21]. The EE of OFDM-IM is studied in [22], where a superior performance compared to classical OFDM is revealed. Based on the minimum Euclidean distance (MED) criterion, a subcarrier allocation scheme assuming channel state information at the transmitter is tailed to OFDM-IM in [23]. To prevent from detecting an illegal SAP in OFDM-IM, all possible SAPs are encoded by varying the modulation order with a specific SAP in [24]. In [25], the transmit diversity of OFDM-IM is improved from unity to two according to the coordinate interleaved orthogonal design principle. The BER performance of OFDM-IM subject to carrier frequency offset (CFO) in fading channels is investigated in [26], which shows that OFDM-IM outperforms classical OFDM in the presence of CFO. The potential of OFDM-IM with inter-carrier interference (ICI) mitigation is explored in [27] and its adaptation to high-mobility scenarios, such as vehicular-to-infrastructure (V2X) [19] and underwater acoustic communications [27], are investigated. The achievable performance of OFDM-IM in terms of MED, average mutual information, and peak-to-average power ratio is analyzed in [28].

This paper aims at increasing the SE and potentially the EE of classical OFDM, or equivalently improving the BER performance at no cost of SE and transmission power, based on the IM principle with a focus on the frequency domain. We note that so far, there have been some efforts to this end in the literature. In [27], an additional bit is introduced as an indicator for the transmission method such that different subcarrier groups can independently make a selection between OFDM-IM or OFDM transmissions. In [29] and [30], OFDM-IM is further combined with the multiple-input multiple-output (MIMO) transmission technique to form MIMO-OFDM-IM, which obtains a linear increase of the SE compared with OFDM-IM. In [31], low-complexity near-ML detection algorithms are proposed for the scheme of MIMO-OFDM-IM. In [32], a compressed sensing (CS) assisted signaling strategy is proposed to enlarge the index domain of OFDM-IM, where a virtual vector of size much larger than that of a subcarrier group is introduced for carrying very few number of modulated symbols, which can be recovered efficiently via CS algorithms. However, the computational complexity is shown to be much higher than that of OFDM-IM. In [33], two variants of OFDM-IM are proposed, including OFDM with generalized index modulation (OFDM-GIM) that allows an adjustable number of active subcarriers, and OFDM with in-phase/quadrature index modulation (OFDM-I/Q-IM) that expands the index domain to include both the in-phase (I-) and quadrature (Q-) dimensions. Theoretical analyses verify that OFDM-I/Q-IM demonstrates more than 6dB and 3dB signal-to-noise ratio (SNR) gains over classical OFDM and OFDM-IM, respectively [17]. However, similar to all aforementioned OFDM-IM related schemes, both OFDM-GIM and OFDM-I/Q-IM deactivate some subcarriers, which do not carry any information by themselves, for IM purposes. In [34], the "inactive" subcarriers of OFDM-IM are allowed to transmit modulated symbols drawn from a secondary constellation that is distinguishable from the primary constellation used by the "active" subcarriers, enlarging the symbol domain significantly while keeping the index domain unchanged. This scheme, called dual-mode IM aided OFDM (DM-OFDM) in [34], is shown to achieve a larger MED than OFDM-IM under the same average bit energy. Actually, if we treat the idle state of a subcarrier or its I/Q branch as a null mode, all OFDM-IM related schemes described above should fall into the dual-mode transmission family. Therefore, it is not surprising to see that the number of all possible transmission patterns excluding the effect of classical modulation is limited to a combinatorial increase. However, the DM-OFDM scheme cleverly overcomes the main limitation of OFDM-IM by transmitting symbols from all available subcarriers along with IM.

Against this background, we propose a novel IM technique applicable to OFDM systems, termed *multiple-mode OFDM-IM (MM-OFDM-IM)*. Our main contributions are summarized as follows.

- In MM-OFDM-IM, all subcarriers are activated to transmit modulated symbols that drawn from different signal constellations (or modes, alternatively). Moreover, the full permutations of these distinguishable modes are utilized for IM purposes, enabling a factorial increase of the number of all possible transmission patterns excluding the effect of classical modulation. The extension of this idea to the I- and Q- branches of OFDM signals, which corresponds to the scheme of MM-OFDM-IM-IQ, is further discussed.[1] This scheme doubles the number of

[1]Note that one can also extend the idea of MM-OFDM-IM to a variable number of modes similar to the extension of OFDM-IM to OFDM-GIM [33]. Here, we only consider the extension to independent IM of I- and Q- branches mainly because decouping the I- and Q- branches adds another degree of freedom, which leads to a faster increase of the SE, and results in a real signal model, which naturally allows us to elaborate on the mode selection from a real signal constellation.

IM bits compared to MM-OFDM-IM with the same system parameters.

- For MM-OFDM-IM(-IQ), an easy-to-implement one-to-one mapping method between the IM bits and mode permutations is provided and the optimal mode selection strategy based on the commonly used phase shift keying (PSK)/quadrature amplitude modulation (QAM)/pulse amplitude modulation (PAM) constellations is designed. The optimal ML receivers, which can be performed via a novel Viterbi-like algorithm searching for possible mode permutations, are proposed. Low-complexity sub-optimal receivers that detect the activated modes subcarrier by subcarrier in an order considering the sub-channel quality are also designed.
- A tight upper bound on the BER of MM-OFDM-IM(-IQ) systems assuming ML detection is derived in closed form. The BER performance of MM-OFDM-IM(-IQ) is further compared with that of the existing state-of-the-art OFDM-IM family members through Monte Carlo simulations, where prominent gains are found. It is also shown that for MM-OFDM-IM, QAM is more favorable than PSK in the high SNR region except for the case that the number of constellation points carried by a mode is no larger than four.

The rest of this paper is outlined as follows. Section II introduces the transceiver structure of MM-OFDM-IM. Mode selection strategies for MM-OFDM-IM, which are constrained on the PSK and QAM constellations, are designed in Section III, followed by the discussion on the selection of system parameters. Section IV discusses the extension of MM-OFDM-IM to the I/Q dimensions, namely MM-OFDM-IM-IQ. Both low-complexity ML and subcarrier-wise detectors are designed, followed by the analysis for the BER upper bound in Section V. Computer simulation results are given in Section VI. Finally, Section VII concludes the paper.

Notation: Upper and lower case boldface letters denote matrices and column vectors, respectively. Superscripts ^{T}, ^{H}, and $^{-1}$ stand for transpose, Hermitian transpose, and matrix inversion operations, respectively. rank($\mathbf{X}$) returns the rank of a matrix $\mathbf{X}$. diag($\mathbf{x}$) creates a diagonal matrix whose diagonal elements are $\mathbf{x}$. $\mathbf{I}_n$ denotes the identity matrix of dimensions $n \times n$. $\Re\{\cdot\}$ and $\Im\{\cdot\}$ return the real and imaginary parts of the argument, respectively. The probability of an event is denoted by $\Pr(\cdot)$. $X \sim \mathcal{CN}(0, \sigma_X^2)$ represents the distribution of a circularly symmetrical complex Gaussian random variable X with variance σ_X^2. $\lfloor\cdot\rfloor$ and $\lceil\cdot\rceil$ denote the floor and the ceiling operations, respectively. $C(\cdot,\cdot)$ denotes the binomial coefficient. $Q(\cdot)$ denotes the tail probability of the standard Gaussian distribution.

II. System Model of MM-OFDM-IM

MM-OFDM-IM is built on an OFDM system of N subcarriers, whose transmitter structure is depicted in Fig. 1. At each time instant, a number of m bits arrive to the transmitter and are equally split into g blocks, each containing $m/g = p$ bits. Since each bit block has the same processing procedure, for brevity, we thereafter take the β-th block as a demonstrative

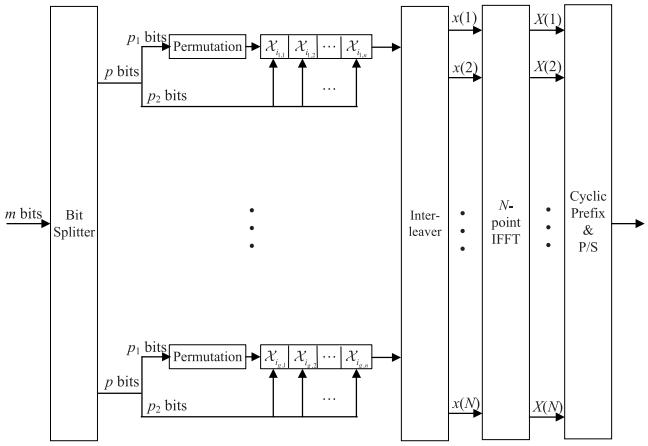

Fig. 1. Block diagram of the MM-OFDM-IM transmitter.

TABLE I
A Look-Up Table Example for $p_1 = 2$ and $n = 3$.

p_1 bits	$\mathcal{I}^{(\beta)}$	Selected modes
[0 0]	$\{1,2,3\}$	$\{\mathcal{X}_1,\mathcal{X}_2,\mathcal{X}_3\}$
[0 1]	$\{1,3,2\}$	$\{\mathcal{X}_1,\mathcal{X}_3,\mathcal{X}_2\}$
[1 0]	$\{2,1,3\}$	$\{\mathcal{X}_2,\mathcal{X}_1,\mathcal{X}_3\}$
[1 1]	$\{3,2,1\}$	$\{\mathcal{X}_3,\mathcal{X}_2,\mathcal{X}_1\}$

example, where $\beta \in \{1,\ldots,g\}$. These p bits are separated into two parts for different purposes: The first part, comprised of p_1 bits, determines the order of the modes $\{\mathcal{X}_1,\ldots,\mathcal{X}_n\}$ that to be employed by n individual subcarriers, where $n = N/g$ and $\mathcal{X}_\gamma$ with $\gamma \in \mathcal{W}(= \{1,\ldots,n\})$ is an M-ary signal constellation, which is assumed to be distinguishable across γ, and the average symbol power of $\{\mathcal{X}_1,\ldots,\mathcal{X}_n\}$ is normalized to unity; the second part, comprised of $p_2 = n\log_2(M)$ bits, generates n symbols $s_1^{(\beta)},\ldots,s_n^{(\beta)}$ that to be transmitted over those subcarriers from the selected modes. To enable IM for the selection of different modes for different subcarriers, we require that the selected n modes must be different from each other, which means the outcome of the p_1 bits can only determine the order set $\{\mathcal{X}_{i_1^{(\beta)}},\ldots,\mathcal{X}_{i_n^{(\beta)}}\}, i_\gamma^{(\beta)} \in \mathcal{W}$, which forms the full permutation of $\mathcal{X}_1,\ldots,\mathcal{X}_n$. Since there are a maximum of $n!$ possible full permutations, it follows that $p_1 = \lfloor\log_2(n!)\rfloor$. The mapping of the p_1 bits to the permutation indices $I^{(\beta)} = \{i_1^{(\beta)},\ldots,i_n^{(\beta)}\}$ can be implemented by either a look-up table or permutation methods, as described below.

1) *Look-Up Table Method:* In this mapping method, a look-up table of size 2^{p_1} is created and used at both the transmitter and receiver sides. For the implementation, the transmitter maps the incoming p_1 bits to a permutation from the table and a reverse operation is performed at the receiver. An example for $p_1 = 2$ and $n = 3$ is presented in Table I. Since $3! = 6$, two permutations out of six are discarded. Explicitly, this mapping method is very efficient; however, it becomes impractical for large values of p_1 due to excessive storage demand.
2) *Permutation Method:* This method provides a one-to-one mapping between integers belonging to $[0, n! - 1]$ and permutations of the elements of $\mathcal{W}$ in lexicographical

order [13]. Details on its implementation are presented in the sequel. First, given an integer $K \in [0, n!-1]$, we can always find a sequence $\jmath = \{c_n, \ldots, c_1\}$, where $c_\gamma \in \mathcal{W}, \gamma \in \mathcal{W}$, to represent it according to $K = (c_n - 1)\cdot(n-1)! + \cdots + (c_2-1)\cdot 1! + (c_1-1)\cdot 0!$, where c_n is the maximum integer that satisfies $(c_n-1)\cdot(n-1)! \le K$, c_{n-1} is the maximum integer satisfying $(c_{n-1}-1)\cdot(n-2)! \le K-(c_n-1)\cdot(n-1)!$, and so on. As an example, for $n=3$, the following $\jmath$ sequences can be calculated:

$$\begin{aligned}
&0 = (1-1)\cdot 2! + (1-1)\cdot 1! + (1-1)\cdot 0! \rightarrow \\
&\jmath = \{1,1,1\} \rightarrow I^{(\beta)} = \{1,2,3\} \\
&1 = (1-1)\cdot 2! + (2-1)\cdot 1! + (1-1)\cdot 0! \rightarrow \\
&\jmath = \{1,2,1\} \rightarrow I^{(\beta)} = \{1,3,2\} \\
&2 = (2-1)\cdot 2! + (1-1)\cdot 1! + (1-1)\cdot 0! \rightarrow \\
&\jmath = \{2,1,1\} \rightarrow I^{(\beta)} = \{2,1,3\} \\
&3 = (2-1)\cdot 2! + (2-1)\cdot 1! + (1-1)\cdot 0! \rightarrow \\
&\jmath = \{2,2,1\} \rightarrow I^{(\beta)} = \{2,3,1\} \\
&4 = (3-1)\cdot 2! + (1-1)\cdot 1! + (1-1)\cdot 0! \rightarrow \\
&\jmath = \{3,1,1\} \rightarrow I^{(\beta)} = \{3,1,2\} \\
&5 = (3-1)\cdot 2! + (2-1)\cdot 1! + (1-1)\cdot 0! \rightarrow \\
&\jmath = \{3,2,1\} \rightarrow I^{(\beta)} = \{3,2,1\}. \qquad (1)
\end{aligned}$$

Since $1! = 0! = 1$, it is not surprising to observe that the last element of $\jmath$, i.e., c_1, always equals 1. Then, according to a $\jmath$ sequence, we can readily determine a permutation $I^{(\beta)}$ by letting $i_1^{(\beta)}$ be the c_n-th element of $\mathcal{W}$, $i_2^{(\beta)}$ be the c_{n-1}-th element of the new set formed by excluding the c_n-th element from $\mathcal{W}$, and so on. For the previous example of $n=3$, all $I^{(\beta)}$ sequences are given in (1). From the above principle, the transmitter first converts the incoming p_1 bits into an integer K, then obtains $\jmath$, and finally $I^{(\beta)}$ from (1), whereas the receiver follows the reverse process. Explicitly, this method incurs a little computational burden; however, it successfully avoids a storage at both the transmitter and receiver, and therefore, is preferred over the look-up table method for large values of p_1.

From above description, when a permutation $I^{(\beta)}$ is determined, we will have $s_\gamma^{(\beta)} \in \mathcal{X}_{i_\gamma^{(\beta)}}$ for $\gamma = 1, 2, \ldots, n$. After obtaining $\{s_\gamma^{(\beta)}\}$ for all β and γ, a block-type interleaver follows, which reads them row-by-row, yielding $\mathbf{S} = [\mathbf{s}^{(1)}, \ldots, \mathbf{s}^{(g)}]^T$, where $\mathbf{s}^{(\beta)} = [s_1^{(\beta)}, \ldots, s_n^{(\beta)}]^T$, and writes them column-by-column, to obtain the $N \times 1$ main OFDM block

$$\begin{aligned}
\mathbf{x}_F &\triangleq [x(1), \ldots, x(N)]^T \\
&= \left[s_1^{(1)}, s_1^{(2)}, \ldots, s_1^{(g)}, \ldots, s_n^{(1)}, s_n^{(2)}, \ldots, s_n^{(g)}\right]^T. \qquad (2)
\end{aligned}$$

From (2), the symbols generated by the β-th bit block are spread to equally spaced subcarriers of indices $\Phi^{(\beta)} = \{\beta, \ldots, \beta + (n-1)g\}$, from which a frequency diversity is expected [18].

At this point, the remaining operations are the same as those of classical OFDM systems. First, the OFDM block is fed into an N-point inverse fast Fourier transform (FFT) module, outputting the time-domain OFDM block $\mathbf{x}_T \triangleq [X(1), X(2), \ldots, X(N)]^T = \frac{1}{\sqrt{N}}\mathbf{W}_N^H \mathbf{x}_F$, where $\mathbf{W}_N$ is the N-point discrete Fourier transform (DFT) matrix with $\mathbf{W}_N^H \mathbf{W}_N = N\mathbf{I}_N$. Then, a length-$P$ cyclic prefix (CP) of samples $[X(N-P+1), \ldots, X(N)]^T$ is appended to the beginning of $\mathbf{x}_T$. Finally, after parallel to serial (P/S) and digital-to-analog conversion, the signal is transmitted.

Consider a slowly time-varying multipath Rayleigh fading channel, which can be modeled by a channel impulse response (CIR) $\mathbf{h}_T \triangleq [h_T(1), \ldots, h_T(\upsilon)]^T$, where υ is the number of channel taps, and $h_T(\sigma), \sigma = 1, \ldots, \upsilon$ are circularly symmetric complex Gaussian random variables (RVs) with the distribution $\mathcal{CN}(0, \delta_\sigma^2)$, where $\sum \delta_\sigma^2 = 1$. Assume that the CP length P is no smaller than the number of channel taps υ. After the removal of the CP from the received signal and the application of N-point FFT, the frequency-domain received signal vector can be derived as

$$\mathbf{y}_F \triangleq [y_F(1), y_F(2), \ldots, y_F(N)]^T = \mathbf{X}\mathbf{h}_F + \mathbf{w}_F \qquad (3)$$

where $\mathbf{X}$ is an $N \times N$ diagonal matrix whose main diagonal elements are given by $x(1), \ldots, x(N)$, $\mathbf{h}_F \triangleq [h_F(1), \ldots, h_F(N)]^T$ is the $N \times 1$ frequency-domain channel vector with the distribution $\mathcal{CN}(0, \mathbf{I}_N)$, and $\mathbf{w}_F$ is the noise vector in the frequency domain with the distribution $\mathcal{CN}(0, N_0\mathbf{I}_N)$. Note that the frequency-domain channel vector is related with the CIR by $\mathbf{h}_F = \mathbf{W}_N \mathbf{h}_T^0$, where $\mathbf{h}_T^0$ is the zero-padded version of the vector $\mathbf{h}_T$ with length N, namely $\mathbf{h}_T^0 = [\mathbf{h}_T, 0, \ldots, 0]^T$. From (3), we can define the average receive SNR per subcarrier as $\rho = 1/N_0$. Explicitly, from above description, the SE of the MM-OFDM-IM system excluding the CP expense can be shown to be (4) (bps/Hz), shown at the top of the next page, where $e = 2.7183$ is the Euler's number, the first approximation is based on the Stirling's Formula $n! \approx \sqrt{2\pi n} n^n e^{-n}$, and the second approximation applies to large values of n. It is indicated in (4) that invoking n modes in MM-OFDM-IM results in an improvement of SE with $\log_2(n/e)$ approximately, which equivalently enlarges the symbol constellation by n/e times, in comparison with classical OFDM.

Since the encoding processes for all bit blocks are independent, the detection for the mode permutation and modulated symbols can be performed block by block without incurring any performance loss. To show this, let $\mathbf{y}_F^{(\beta)} = \Pi^{(\beta)}\mathbf{y}_F$, $\mathbf{h}_F^{(\beta)} = \Pi^{(\beta)}\mathbf{h}_F$, $\mathbf{s}^{(\beta)} = \Pi^{(\beta)}\mathbf{s}$, and $\mathbf{X}^{(\beta)} = \mathrm{diag}(\mathbf{s}^{(\beta)})$, where $\Pi^{(\beta)}$ refers to the de-interleaving operation for subblock β, which is an $n \times N$ matrix constructed by the rows of $\mathbf{I}_N$, whose indices belong to $\Phi^{(\beta)}$. In lieu of (3), the receiver can make a joint decision on the two information carrying units for the β-th bit block based on the ML criterion via

$$\left(\mathbf{s}_{est}^{(\beta)}, I_{est}^{(\beta)}\right) = \arg\min_{\mathbf{s}^{(\beta)}, I^{(\beta)}} \left\| \mathbf{y}_F^{(\beta)} - \mathbf{X}^{(\beta)}\mathbf{h}_F^{(\beta)} \right\|^2 \qquad (5)$$

where $I_{est}^{(\beta)} \triangleq [\hat{i}_1^{(\beta)}, \ldots, \hat{i}_n^{(\beta)}]^T$ and $\mathbf{s}_{est}^{(\beta)} \triangleq [\hat{s}_1^{(\beta)}, \ldots, \hat{s}_n^{(\beta)}]^T$. Unfortunately, the computational complexity of the optimal ML detector in (5) in terms of complex multiplications is of order $\sim O(n!M^n)$ per bit block, which becomes impractical

$$\begin{aligned} F_{\text{MM-OFDM-IM}}(M,n) &= \frac{p_1+p_2}{n} = \frac{1}{n}\left\lfloor \log_2(n!) \right\rfloor + \log_2(M) \\ &\approx \frac{1}{n}\left\lfloor n\log_2(n) - n\log_2(e) + \log_2\left(\sqrt{2\pi n}\right)\right\rfloor + \log_2(M) \\ &\approx \log_2(n) - \log_2(e) + \log_2(M) \end{aligned} \tag{4}$$

for large values of n and M. On the other hand, the design of low-complexity detectors will be investigated in Section V.

III. Mode and Parameter Selection for MM-OFDM-IM

The determination of n distinguishable modes $\{\mathcal{X}_1, \ldots, \mathcal{X}_n\}$ while facilitating symbol modulation/demodulation and the selection of system parameters M and n for a given SE value are two crucial issues for MM-OFDM-IM since, as stated in Section II, the permutations of these n modes also carry information. In this section, first, we design the guidelines for mode selection, then, we propose a practical mode selection strategy by partitioning PSK and QAM constellations, and finally, we shed light on how to select the system parameters.

A. Guidelines for Mode Selection

According to (5), the optimal modes, in the sense of the BER performance of MM-OFDM-IM systems at high SNR, should maximize the Euclidean distance (intra-mode distance criterion)

$$\begin{aligned} \lambda_1 &= \min_{\kappa,\nu\in\{1,\ldots,2^p\}} \left\| \mathbf{X}_\kappa^{(\beta)} - \mathbf{X}_\nu^{(\beta)} \right\|_F^2, \\ s.t.\ \ & E\{\|\mathbf{X}^{(\beta)}\|_F^2\} = n,\ \text{rank}\left(\mathbf{X}_\kappa^{(\beta)} - \mathbf{X}_\nu^{(\beta)}\right) = r_{\min} \end{aligned} \tag{6}$$

where $\mathbf{X}_\kappa^{(\beta)}$ and $\mathbf{X}_\nu^{(\beta)}$ are two different realizations of the frequency-domain transmission matrix $\mathbf{X}^{(\beta)}$ and $r_{\min}$ is the diversity order achieved by the system, which is defined as $r_{\min} = \min \text{rank}(\mathbf{X}_k^{(\beta)} - \mathbf{X}_v^{(\beta)})$. Note that we have ignored the channel correlation in (6), which is reasonable as the subcarriers associated with a bit block probably undergo independent fading with the employment of the interleaver at the transmitter. Since the bits for generating $s_1^{(\beta)}, \ldots, s_n^{(\beta)}$ are independent, it can be readily inferred that $r_{\min} = 1$, which implies that the erroneous detection mainly occurs on the modulated symbol drawn from a single mode in the high SNR region. Recall that each mode in MM-OFDM-IM is a different M-ary signal constellation. Since the MED between any two signal points of a fixed-size constellation increases with the average power of the constellation, in lieu of (6), the optimal modes must satisfy a prerequisite that they must have a normalized average power without overlap, namely $\mathcal{X}_{\gamma_1} \cap \mathcal{X}_{\gamma_2} = \emptyset$, $\gamma_1 \neq \gamma_2$, for $\gamma_1, \gamma_2 \in \mathcal{W}$. In [35], the optimal two-dimensional M-ary constellation under an average power constraint has been already determined, whose points lie in the vertices of a trellis of (almost) equilateral triangles and become uniformly distributed on a circle as M goes to infinity. Since the rotation of a constellation does not change its average symbol power and the MED, for finite values of M, the number of optimal constellations are typically much larger than n. Therefore, the optimal n modes satisfying (6) can be directly selected as any n out of those candidates, among which no overlap exists.[2]

The criterion of (6) only focuses on the high SNR region, which, however, does not necessarily guarantee satisfactory BER performance in the medium SNR region. To achieve better BER performance at medium SNR, a feasible approach is to select n solutions out of those provided by (6), which further maximize the Euclidean distance at a diversity order of two (inter-mode distance criterion)

$$\begin{aligned} \lambda_2 &= \min_{\kappa,\nu\in\{1,\ldots,2^p\}} \left\| \mathbf{X}_\kappa^{(\beta)} - \mathbf{X}_\nu^{(\beta)} \right\|_F^2, \\ s.t.\ \ & E\{\|\mathbf{X}^{(\beta)}\|_F^2\} = n,\ \text{rank}\left(\mathbf{X}_\kappa^{(\beta)} - \mathbf{X}_\nu^{(\beta)}\right) = 2. \end{aligned} \tag{7}$$

The second constraint in (7) requires us to take into account the errors that arise from either mistaking the permutation of any two modes or erroneously demodulating two symbols drawn from their respective modes. For those solutions of (6) maximizing the minimum distance between any two signal points of a mode, which is called the minimum intra-mode distance (MIAD), the probability of error caused by the latter is commonly much smaller than that by the former. Therefore, the criterion of (7) is equivalent to filtering the solutions of (6), leaving those maximizing the minimum distance between any two signal points of two modes, which is called the minimum inter-mode distance (MIRD).

As an example of $M = 2$, the optimal eight modes determined according to the aforementioned guidelines are depicted in Fig. 2. Details on the mode selection are explained as follows. First, we pick up the BPSK constellation, as it is well known to be the optimal signal constellation for $M = 2$. Then, by rotating it with different angles, we obtain multiple different modes, out of which any n modes result in the maximum MIAD. Finally, we select those generated with rotation angles $\pi(\gamma - 1)/n, \gamma = 1, \ldots, n$ as the output, which have the maximum MIRD and construct a virtual $2n$-PSK constellation. Therefore, in this example of $n = 8$, we obtain a 16-PSK constellation in Fig. 2. At this point, let us extend this example to larger values of M. For $M = 4$, the 4-PSK constellation is optimum [35]. In a similar manner, we can deduce that the optimal n modes for $M = 4$ are the n rotated versions of the 4-PSK constellation with rotation

[2]For the special case that M is not an integer power of two, the optimal constellation may include a zero point [35], for which any rotation cannot generate a non-overlapping constellation, and as a result, a complicated computer search for the optimal n modes is needed. Fortunately, this problem can be avoided in practice, since we usually choose M to be an integer power of two to ensure an integral number of bits per modulated symbol.

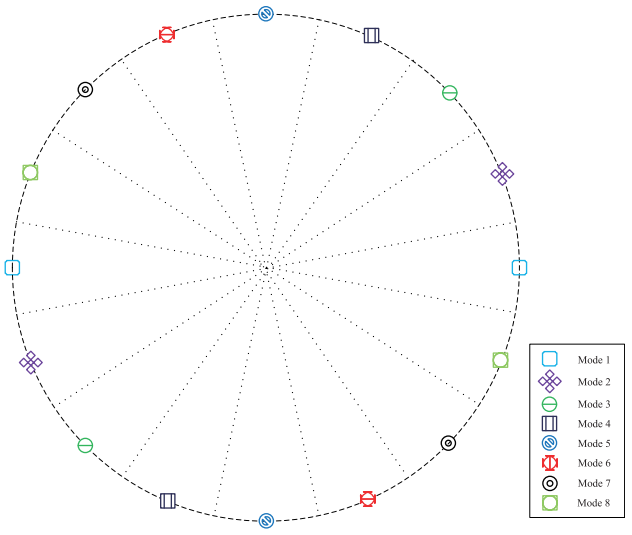

Fig. 2. Eight optimal modes generated from the 16-PSK constellation, where each mode carries one bit and is distinguished by its decision zone.

angles $\pi(\gamma-1)/2n, \gamma=1,\ldots,n$, which as a whole should construct the $4n$-PSK constellation. For example, in the case of $n=4$, a combined 16-PSK constellation is formed by the optimal four modes $\{x_1^*, x_5^*\}, \{x_2^*, x_6^*\}, \{x_3^*, x_7^*\}, \{x_4^*, x_8^*\}$, where $x_\gamma^*, \gamma=1,\ldots,8$ are the optimal eight modes for $M=2$ obtained from the previous example in Fig. 2. For $M>4$, a non-regular Mn-ary constellation will be constructed by the n optimal modes; however, they are not conventional and efficient signaling formats, such as PSK and QAM constellations [35]. This is undesirable since in practice, we would prefer a regular constellation over a non-regular one for its lower symbol modulation/demodulation complexity at the cost of a marginal performance loss, which is shown to be as high as 0.5dB in [35].

B. Practical Mode Selection Strategy

Aiming at a regular Mn-ary constellation, we propose a practical mode selection strategy from PSK and QAM constellations by following the criterions of (6) and (7).

1) PSK Constraint: We begin with the PSK constraint. Explicitly, the basic constellation for generating all modes, denoted by x_0, can be the ordinary M-PSK constellation, whose signals points are located on a circle of unit radius and have a minimum distance separation of

$$d_{intra}^{\mathrm{PSK}}(M)=2\sin\left(\frac{\pi}{M}\right). \tag{8}$$

To maximize the MIRD, it is straightforward to see that the n modes should be uniformly distributed in a circle, which can be generated by rotating x_0 with angles $2\pi(\gamma-1)/Mn, \gamma=1,\ldots,n$. Consequently, these n modes construct the Mn-PSK constellation, whose MIRD becomes the MED of the Mn-PSK constellation, namely

$$d_{inter}^{\mathrm{PSK}}(M,n)=d_{intra}^{\mathrm{PSK}}(Mn)=2\sin\left(\frac{\pi}{Mn}\right) \tag{9}$$

which is a function of M and n, but depends on their product only. It is expected from the analysis in Section III.A that when M equals 2, 4, and a very large value, the best asymptotic BER performance will be achieved by this mode selection strategy since the n modes happen to strike the maximum MIAD. However, since the Mn constellation points are confined on a circle, the BER performance in the lower SNR region will be limited by the MIRD.

2) QAM Constraint: Constrained on a QAM signal constellation, the combined n modes can be only an Mn-QAM constellation, which is assumed to be the combination of the $2^{\lfloor\log_2(\sqrt{Mn})\rfloor}$-PAM and $2^{\lceil\log_2(\sqrt{Mn})\rceil}$-PAM constellations. It can be verified that the resulting MIRD is

$$d_{inter}^{\mathrm{QAM}}(M,n)=\begin{cases}\frac{2\sqrt{6}}{\sqrt{5Mn-4}}, & \text{for rectangular } Mn\text{-QAM}\\ \frac{\sqrt{6}}{\sqrt{Mn-1}}, & \text{for square } Mn\text{-QAM}\end{cases} \tag{10}$$

which, as similar to the PSK constraint, depends on the product of M and n only. Comparing (10) with (9), we observe that $d_{inter}^{\mathrm{QAM}}(M,n) > d_{inter}^{\mathrm{PSK}}(M,n)$ for $Mn>4$. Therefore, it is expected that the QAM constraint will perform better than the PSK constraint in the medium SNR region for $Mn>4$, which is also common in practical use. Given the Mn-QAM constellation, the n modes can be obtained by partitioning it into n subsets, each corresponding to a mode. Here, attention should be paid to the partitioning method, since a different one may lead to a different MIAD. A straightforward partitioning method is to follow the principle of proximity, based on which the closest M constellation points are grouped into a mode, yielding an M-QAM constellation. However, it is not recommended since the resulting MIAD is limited to the MED of the Mn-QAM constellation, which is the same as the MIRD in (10). The best partitioning method should maximize the MIAD. From this point of view, it can be found that our aim is similar to that of the famous trellis coded modulation (TCM) set partitioning technique [36], whose idea is to expand the signal set to increase the MED between the pairs of coded signals. It has been disclosed in [36] that the optimal n subsets can be obtained by $\log_2(n)$ levels of set partitioning, each increasing the MED by $\sqrt{2}$. However, we note that this property is valid for most cases except for an Mn-ary rectangular constellation with $M=2$, for which the last partitioning should increase the MED by $\sqrt{5/2}$ instead due to the imbalance between the I- and Q- branches. Consequently, the MIAD can be calculated by (11), shown at the bottom of the next page.

To verify the above analysis, we present two examples under the Mn-QAM constraint with $Mn=16$ and 8, respectively, in Figs. 3 and 4, where the optimal n modes for $M=2$ are also depicted. The MIRDs can be easily calculated from (10) as $d_{inter}^{\mathrm{QAM}}(2,8)=2/\sqrt{10}=0.6325$ and $d_{inter}^{\mathrm{QAM}}(2,4)=2/\sqrt{6}=0.8165$, respectively. The MIAD seems a little more difficult to explain since it depends on both M and n. For the example in Fig. 3, the MIAD for $M=2$ can be easily calculated from the figure as well as from (11) as $d_{intra}^{\mathrm{QAM}}(2,8)=4/\sqrt{5}=1.7889$. The optimal $n=4$ modes for $M=4$ can be directly obtained from the optimal eight modes $x_\gamma^*, \gamma=1,\ldots,8$ for $M=2$ by combining x_1^* and x_5^*, x_2^* and x_6^*, x_3^* and x_7^*, as well as x_4^* and x_8^*, resulting in an MIAD of $d_{intra}^{\mathrm{QAM}}(4,4)=4/\sqrt{10}=1.2649$. Similarly, the optimal $n=2$ modes for $M=8$ are

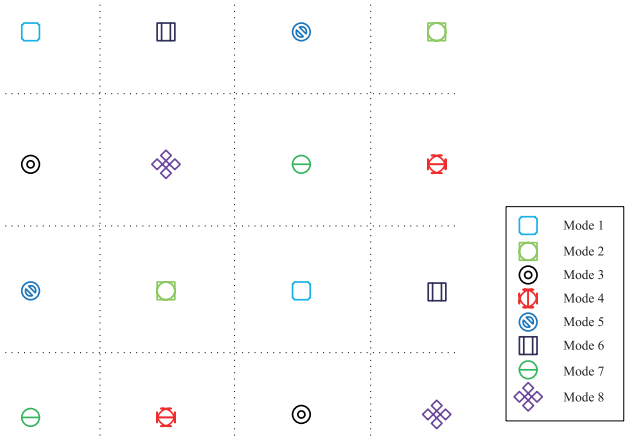

Fig. 3. Eight optimal modes generated from the 16-QAM constellation, where each mode carries one bit and is distinguished by its decision zone.

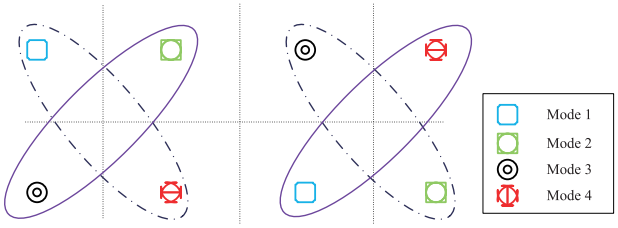

Fig. 4. Four optimal modes generated from the 8-QAM constellation, where each mode carries one bit and is distinguished by its decision zone. For $M = 4$, the two optimal modes are included by the dash-dot and solid ellipses.

$\{x_1^*, x_4^*, x_5^*, x_8^*\}$ and $\{x_2^*, x_3^*, x_6^*, x_7^*\}$, which have an MIAD of $d_{intra}^{\mathrm{QAM}}(8,2) = 2/\sqrt{5} = 0.8944$. On the other hand, for the example in Fig. 4, the MIAD for $M = 4$ can be easily calculated from the figure as $d_{intra}^{\mathrm{QAM}}(4,2) = 2/\sqrt{3} = 1.1547$. However, unlike the example in Fig. 3, these two optimal modes should not be partitioned into four modes, since in this way, the resulting MIAD is only $\sqrt{2}$ times of $d_{intra}^{\mathrm{QAM}}(4,2)$. The optimal four modes for $M = 2$ are shown in Fig. 4, which gain $\sqrt{5/2}$ times of MED, namely the MIAD is $d_{intra}^{\mathrm{QAM}}(2,4) = \sqrt{5/2} d_{intra}^{\mathrm{QAM}}(4,2) = 2\sqrt{5}/\sqrt{6} = 1.8257$.

Actually, at larger SEs for the MM-OFDM-IM systems, we usually have $Mn \gg 1$ from (4). With this property, it can be inferred from (11) that the MIAD under the QAM constraint approaches to its lower bound

$$d_{intra}^{\mathrm{QAM}}(M,n) \approx d_{intra}^{\mathrm{QAM}}(M) = \begin{cases} 2\sqrt{\frac{6}{5M}}, & \text{for rectangular } Mn\text{−QAM with } M \neq 2 \\ \sqrt{\frac{6}{M}}, & \text{otherwise} \end{cases} \tag{12}$$

which becomes independent of n, as similar to the PSK constraint. Comparing (12) with (8), we observe that $d_{intra}^{\mathrm{QAM}}(M) > d_{intra}^{\mathrm{PSK}}(M)$ for $M > 4$. Therefore, by incorporating the finding after (10), we are led to the conclusion that the QAM constraint is more favorable than the PSK constraint in terms of BER in the medium-to-high SNR region for $M > 4$.

C. Discussion on Parameter Selection

The above subsections focus on the mode selection method for a given pair of M and n. We now shift our focus to the optimal combination of M and n for a given SE value.

To see the effects of M and n on the system's SE, we calculate the corresponding exact SE values for different M and n considering the first line of (4) in Table II. One can see from each column of Table II that doubling M always leads to an increase of 1 bps/Hz. On the other hand, as seen from each row of Table II, doubling n leads to a different increase scale for the SE, which grows with n and is saturated to 1 bps/Hz around $n = 8$. This implies that for $n < 8$, the contribution of ordinary modulation to the SE is more significant than that of IM, while for $n \geq 8$, their contributions are similar. Therefore, it is not surprising to observe that Table II is approximately symmetric for $n \geq 8$, namely the values of M and n are nearly interchangeable for $M \geq 8$ and $n \geq 8$. Note that this property can be also inferred from the last approximation in (4). Despite similar contributions of M and n to the system's SE, the resulting system performance is quite different for a different combination of them under a given constant Mn. As indicated in (8)-(12), although the MIRD remains the same, the MIAD becomes smaller for a larger M. Consequently, the combinations marked with blue color in Table II are preferred over their symmetric counterparts marked with red color in this sense. However, as revealed in (5), the price to pay for this improvement is an increment in the total number of ML metric calculations since n gives rise to a factorial increase while M corresponds to an exponential increase.[3]

IV. Extension to I/Q Dimension

In MM-OFDM-IM, the multiple-mode transmission is carried out through the I- and Q- branches jointly. This is necessary when each mode is two-dimensional and its I- and Q- branches are correlated as well, such as in the PSK constraint. However, for the case of QAM constellations, the I- and Q- branches can be decoupled to realize independent multiple-mode transmission, doubling the number of IM bits.

[3]The same price in complexity is paid if we apply the proposed low-complexity ML detector in Section V.A, as it has a detection complexity of $O(Mn + 2^{n-1})$ per subcarrier. Fortunately, when applying the proposed subcarrier-wise detector in Section V.B, the detection complexity becomes $O(Mn/2 + M/2)$ per subcarrier, and therefore, no price is needed to be paid in terms of the detection complexity.

$$d_{intra}^{\mathrm{QAM}}(M,n) = \begin{cases} d_{inter}^{\mathrm{QAM}}(M,n)\frac{\sqrt{5n}}{2}, & \text{for rectangular } Mn\text{−QAM with } M = 2 \\ d_{inter}^{\mathrm{QAM}}(M,n)\sqrt{n}, & \text{otherwise} \end{cases}. \tag{11}$$

TABLE II
SPECTRAL EFFICIENCIES OF MM-OFDM-IM SYSTEMS VERSUS M AND n (BPS/HZ)

$n=$		2	4	8	16	32	64	128
$M=$	2	1.500	2.000	2.875	3.750	4.6563	5.6094	6.5938
	4	2.500	3.000	3.875	4.750	5.6563	6.6094	7.5938
	8	3.500	4.000	4.875	5.750	6.6563	7.6094	8.5938
	16	4.500	5.000	5.875	6.750	7.6563	8.6094	9.5938
	32	5.500	6.000	6.875	7.750	8.6563	9.6094	10.594
	64	6.500	7.000	7.875	8.750	9.6563	10.609	11.594
	128	7.500	8.000	8.875	9.750	10.656	11.609	12.594

In this section, we first introduce the implementation of this extension, namely MM-OFDM-IM-IQ, and then design the tailored mode-selection strategy.

A. Implementation of MM-OFDM-IM-IQ

For ease of comparison with MM-OFDM-IM, we follow a similar notation to that of Section II. At the transmitter, the incoming m bits for generating an OFDM block are also equally split into g blocks, each consisting of p bits. Let us focus on the β-th bit block, where $\beta \in \{1, \ldots, g\}$. The p bits are divided into two parts, which are comprised of p^I and p^Q bits, respectively, to modulate the I- and Q-branches independently. Let us consider the I-branch. Similar to MM-OFDM-IM, the p^I bits are further separated into $p_1^I = \lfloor \log_2(n!) \rfloor$ bits, which determine a full permutation of n distinguishable M-ary PAM signal constellations $\mathcal{X}_1, \ldots, \mathcal{X}_n$, and $p_2^I = n \log_2(M)$ bits, which generate a symbol vector $\tilde{\mathbf{s}}^{(\beta)} = [\tilde{s}_1^{(\beta)}, \ldots, \tilde{s}_n^{(\beta)}]^T$ with elements drawn from the permuted modes. Specially, the average symbol power of $\{\mathcal{X}_1, \ldots, \mathcal{X}_n\}$ is $1/2$, and all constellation points of the n modes are limited to real numbers. How to relate the p^I bits with the permutation indices, denoted by $\tilde{\mathcal{I}}^{(\beta)} = \{i_{\mathrm{I},1}^{(\beta)}, \ldots, i_{\mathrm{I},n}^{(\beta)}\}$, where $i_{\mathrm{I},\gamma}^{(\beta)} \in \mathcal{W}$, $\gamma \in \mathcal{W}$, has been addressed in Section II, and thus, is omitted here for brevity. The Q-branch is modulated in a similar manner. Denote the output symbol vector of the Q-branch as $\bar{\mathbf{s}}^{(\beta)} = [\bar{s}_1^{(\beta)}, \ldots, \bar{s}_n^{(\beta)}]^T$. After this point, $2n$ output symbols of the I- and Q- branches are combined to obtain $\mathbf{s}^{(\beta)} \triangleq [s_1^{(\beta)}, s_2^{(\beta)}, \ldots, s_n^{(\beta)}]^T = \tilde{\mathbf{s}}^{(\beta)} + j\bar{\mathbf{s}}^{(\beta)}$, which is to be transmitted by the n subcarriers of indices $\Phi^{(\beta)} = \{\beta, \beta+g, \ldots, \beta+(n-1)g\}$ after the interleaving operation. Finally, the OFDM block creator forms the $N \times 1$ main OFDM block by concatenating the outputs of g bit blocks, yielding (2).

The frequency-domain received signal vector can be expressed in the same form as (3). Due to the independence between the I- and Q- branches, it is possible to decouple the overall detection into independent I- and Q- detections. For the I-branch detection, we have

$$\left(\tilde{\mathbf{s}}_{est}^{(\beta)}, \tilde{\mathcal{I}}_{est}^{(\beta)}\right) = \arg\min_{\tilde{\mathbf{s}}^{(\beta)}, \tilde{\mathcal{I}}^{(\beta)}} \left\| \mathbf{H}^{(\beta)} \left(\Re\{\mathbf{z}_F^{(\beta)}\} - \tilde{\mathbf{s}}^{(\beta)} \right) \right\|^2 \quad (13)$$

where $\mathbf{H}^{(\beta)} = \mathrm{diag}(\mathbf{h}_F^{(\beta)})$ and $\mathbf{z}_F^{(\beta)} = \mathbf{H}^{(\beta)-1}\mathbf{y}_F^{(\beta)}$ refers to the frequency-domain equalized signal vector. It can be observed that (13) exhibits the same computational complexity as (5), which, however, is still intolerable despite significant complexity reduction. In Section V, we will solve this problem with practical low-complexity receivers.

From above description, the SE of the MM-OFDM-IM-IQ system can be calculated as (14), shown at the bottom of this page, where the approximation holds for large values of n. Comparing (14) with (4), we can observe that with the same parameters of M and n, the MM-OFDM-IM-IQ system achieves a double SE than the MM-OFDM-IM system.

B. Mode Selection from PAM Constellation

Since given a power constraint, the optimal one-dimensional signal constellation in the sense of maximizing the MED is unique, by following the design guidelines in Section II.A to search for the optimal n modes, we will always obtain a combined non-regular Mn-ary signal constellation formed by different modes. To circumvent this problem, in this subsection, we propose a practical mode selection strategy based on the conventional one-dimensional efficient signaling format, namely the PAM constellation.

Constrained on a combined Mn-PAM constellation of unit power, the MIRD is given by

$$d_{inter}^{\mathrm{PAM}}(M, n) = \frac{2\sqrt{3}}{\sqrt{(Mn)^2 - 1}} \quad (15)$$

which depends on the value of Mn only. Then, aiming at the maximum MIAD, we resort to the principle of set partitioning to select the n modes. Specifically, we first divide the Mn-PAM constellation into two subsets by assigning alternate points to each subset, and then further divide each subset into two smaller ones by assigning alternate points to each of them, and so on until n subsets are obtained. Since the entire process includes $\log_2(n)$ levels of partitioning and each increases the MED by a factor of 2, the resulting MIAD is

$$d_{intra}^{\mathrm{PAM}}(M, n) = \frac{2\sqrt{3}}{\sqrt{M^2 - n^{-2}}} \approx d_{intra}^{\mathrm{PAM}}(M) = \frac{2\sqrt{3}}{M} \quad (16)$$

where the approximation holds for large values of n. An example of $M = 2$ and $n = 4$ is given in Fig. 5, where the four

$$\begin{aligned} \digamma_{\mathrm{MM-OFDM-IM-IQ}}(M, n) &= \frac{p^I + p^Q}{n} = \frac{2}{n}\left\lfloor \log_2(n!) \right\rfloor + 2\log_2(M) \\ &\approx 2\log_2(n) - 2\log_2(e) + 2\log_2(M) \end{aligned} \quad (14)$$

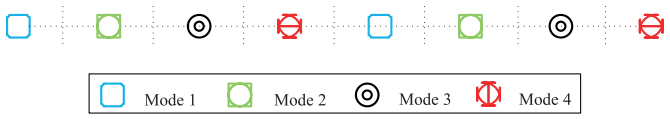

Fig. 5. Four optimal modes generated from the 8-PAM constellation, where each mode carries one bit and is distinguished by its decision zone.

optimal modes $\mathcal{X}_1^*, \ldots, \mathcal{X}_4^*$ are shown. In this example, the MIAD and MIRD can be readily calculated as $d_{intra}^{\text{PAM}}(2,4) = 8/\sqrt{21} = 1.7457$ and $d_{inter}^{\text{PAM}}(2,4) = 2/\sqrt{21} = 0.4364$, respectively. For $M = 4$ and $n = 2$, the optimal two modes are the combination of $\mathcal{X}_1^*$ and $\mathcal{X}_3^*$, as well as $\mathcal{X}_2^*$ and $\mathcal{X}_4^*$, which lead to MIAD and MIRD of $d_{intra}^{\text{PAM}}(4,2) = 4/\sqrt{21} = 0.8729$ and $d_{inter}^{\text{PAM}}(4,2) = 2/\sqrt{21} = 0.4364$, respectively.

V. Receiver Design and Performance Analysis

In this section, we propose two low-complexity detectors for MM-OFDM-IM(-IQ) systems. The first one employs a novel Viterbi-like algorithm to significantly reduce the search space for all possible mode permutations based on the optimal ML detection, and the second one performs detection subcarrier-wise considering the sub-channel quality, which exhibits near optimal performance with very low computational complexity especially at high SNR. We further provide a tight upper bound on the ultimate BER of MM-OFDM-IM(-IQ) systems. Since the detection for each bit block is similar and independent as well, we will only focus on the β-th bit block for analysis and omit the superscript (β) to simplify notations.

A. Low-Complexity Detectors

This subsection introduces the principles of the proposed low-complexity detectors. Since as indicated in Section IV.A, the detection of the MM-OFDM-IM-IQ signal can be decoupled into independent I- and Q- signal detections, both of which are similar to the detection of the MM-OFDM-IM signal, we take the MM-OFDM-IM signal detection as a demonstrative example.

1) Low-Complexity ML Detector: Let us consider an $n \times n$ matrix $\mathbf{G}$, whose (ς, τ)-th entry refers to the most-likely conveyed symbol when the ς-th subcarrier employs $\mathcal{X}_\tau$

$$G_{\varsigma,\tau} = \arg\min_{s \in \mathcal{X}_\tau} |y_F(\varsigma) - s \cdot h_F(\varsigma)|^2, \ \varsigma, \tau \in \mathcal{W}. \quad (17)$$

Further, let us consider another $n \times n$ matrix $\mathbf{T}$ with $T_{\varsigma,\tau} = \left|y_F(\varsigma) - G_{\varsigma,\tau} h_F(\varsigma)\right|^2$, which stores the optimum decision metrics. From (5), the indices of the permuted modes can be estimated via

$$I_{est} = \arg\min_{I} \sum_{\gamma=1}^{n} T_{\gamma,i_\gamma} \quad (18)$$

and given I_{est}, the most-likely symbols carried on the n subcarriers can be directly obtained from $\mathbf{G}$ as $\mathbf{s}_{est} = [G_{1,\hat{i}_1}, \ldots, G_{n,\hat{i}_n}]^T$. Explicitly, the overall computational complexity of (17) and (18) is of order $\sim \mathcal{O}(Mn^2 + n!)$, which is considerably lower than that of the brute-force search ($\sim \mathcal{O}(M^n n!)$). However, it is still intolerable when n goes large, since the part contributed by the search for the permutation indices becomes dominant and increases factorially with n. Noticing that the summation in (18) has memory, we are motivated by the Viterbi algorithm [37], [38] to reduce the search space.

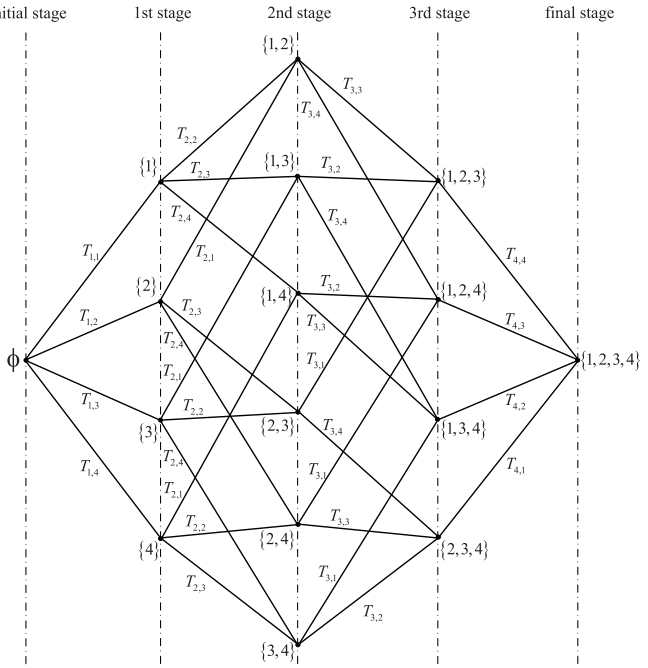

Fig. 6. Trellis diagram for $n = 4$ used for the detection of the order of the considered modes.

To apply the proposed detection algorithm, it is necessary to initiate a trellis in analogy with the Viterbi algorithm. According to (18), a possible trellis should have $n+1$ stages so that n state transitions are available for accumulating the n metrics $T_{1,i_1}, \ldots, T_{n,i_n}$. In the trellis, the initial state is labeled by an empty set $\emptyset$, which indicates that no mode is employed by any subcarrier, and at the γ-th stage, there are in total $C(n,\gamma)$ states labeled by the γ-combinations of n modes, which correspond to all possible modes employed by the first γ subcarriers without considering the mode permutation, where $\gamma \in \mathcal{W}$. A path exists if the label of its connecting node (namely the state) at the $(\gamma-1)$-th stage is a subset of the label of its another connecting node at the γ-th stage, and it is associated with a path metric $T_{\gamma,\xi}$, where ξ is the complementary mode index. Therefore, according to the above labeling rule, each node at the γ-th stage will have γ incoming and $n-\gamma$ outgoing paths. For better understanding, we plot the corresponding trellis diagram for $n = 4$ in Fig. 6. After the initiation of the trellis, the decoding in (18) is equivalent to finding a path that stems from the initial state and terminates at the final state with the minimum additive metric. Resorting to the idea of the Viterbi algorithm, we compare the accumulated metrics for all paths that merge at a node and keep the one with the minimum value only for further consideration. Moreover, when this surviving path is determined, the label of the merged node is updated with the mode permutation information it carries. For example, consider the two paths in the trellis of

TABLE III
COMPARISON OF DETECTION COMPLEXITY BETWEEN MM-OFDM-IM AND CLASSICAL OFDM

	MM-OFDM-IM			Classical OFDM
	ML	Low-Complexity ML	Subcarrier-Wise	ML (M'-PSK/QAM)
$(M,n)=(2,4),\quad M'=4$	96	16	5	4
$(M,n)=(2,8),\quad M'=7$	1.29×10^{6}	144	9	7
$(M,n)=(4,8),\quad M'=14$	3.30×10^{8}	160	18	14
$(M,n)=(8,8),\quad M'=29$	8.46×10^{10}	192	36	29
$(M,n)=(16,16),M'=107$	2.41×10^{31}	33024	136	107

Fig. 6 that begin at the initial state $\emptyset$ and remerge at state $\{1,2\}$ after two state transitions. If the accumulated metric for the upper path, namely $T_{1,1}+T_{2,2}$, is smaller than that for the lower path $T_{1,2}+T_{2,1}$, the label of the state is updated with $\{1,2\}$, or $\{2,1\}$ otherwise. The above procedure is repeated until the final state is arrived, whose updated label provides the most probable permuted indices I_{est}. Since each path that converges at a common node requires the computation of a metric, γ metrics are computed for each node at the γ-th stage. Since there are $C(n,\gamma)$ states at the γ-th stage as mentioned before, the total number of computations in decoding is of order $\sim O(\sum_{\gamma=1}^{n}\gamma\, C(n,\gamma)) = O(n2^{n-1})$, which is much less than that required in (18).

2) Subcarrier-Wise Detector: Despite great efforts, the computational complexity of the proposed low-complexity ML detector is still dominated by the part stemming from the search for the mode permutation as n gets higher. To achieve a much lower computational complexity, we design a suboptimal subcarrier-wise detector, which dispenses with this search.

From the principle of multiple-mode transmission, any one out of the n modes is likely to be employed by the ς-th subcarrier, whose probability can be measured by an LLR value

$$L_{\varsigma,\tau} = \ln\frac{\Pr(\mathrm{E}|\, y_F(\varsigma))}{\Pr(\mathrm{E}_\perp|\, y_F(\varsigma))} \propto \ln\frac{\sum_{s\in\mathcal{X}_\tau}\exp\left(-\rho|y_F(\varsigma)-s\cdot h_F(\varsigma)|^2\right)}{\sum_{\gamma\neq\tau}\sum_{s\in\mathcal{X}_\gamma}\exp\left(-\rho|y_F(\varsigma)-s\cdot h_F(\varsigma)|^2\right)} \quad (19)$$

where E represents the event that the ς-th subcarrier employs $\mathcal{X}_\tau$ and $\mathrm{E}_\perp$ is the complement of E. By the definition in (19), a larger LLR value means that the ς-th subcarrier is more likely to employ $\mathcal{X}_\tau$. Let us construct an $n\times n$ matrix $\mathbf{L}$ by taking $L_{\varsigma,\tau}$ of (19) as its (ς,τ)-th entry. The proposed subcarrier-wise detector operates in the following three steps:

- Sort the channels of the n subcarriers according to the absolute values of their coefficients in decreasing order, which means, if $|h_F(q_1)|^2 \geq \cdots \geq |h_F(q_n)|^2$, where $q_\gamma, \gamma\in\mathcal{W}$, the output is $\mathcal{Q}=\{q_1,\ldots,q_n\}$.
- Determine the modes carried on the n subcarriers by following the order dictated in $\mathcal{Q}$. Specifically, we start with the q_1-th subcarrier, whose conveying mode is estimated as the one resulting in the maximum LLR value among the n modes $\{\mathcal{X}_1,\ldots,\mathcal{X}_n\}$, denoted by $\mathcal{X}_{\hat{i}_{q_1}}$, and then we move on to the q_2-th subcarrier, whose conveying mode is estimated as $\mathcal{X}_{\hat{i}_{q_2}}$, which is associated with the maximum LLR value among the remaining $n-1$ modes $\{\mathcal{X}_1,\ldots,\mathcal{X}_n\}\backslash\mathcal{X}_{\hat{i}_{q_1}}$, and so on until the q_n-th subcarrier is reached, whose conveying mode is estimated as the sole element of $\{\mathcal{X}_1,\ldots,\mathcal{X}_n\}\backslash\{\mathcal{X}_{\hat{i}_{q_1}},\ldots,\mathcal{X}_{\hat{i}_{q_{n-1}}}\}$, denoted by $\mathcal{X}_{\hat{i}_{q_n}}$.
- Determine the symbols conveyed by the n subcarriers. The outputs are obtained as $\mathbf{s}_{est}=[G_{1,\hat{i}_1},\ldots,G_{n,\hat{i}_n}]^T$, where the elements are given by (17).

Actually, since the constellation points of each mode are equally distributed over the combined Mn-PSK/QAM constellation, the LLR value in (19) can be well approximated by

$$L_{\varsigma,\tau}\approx\ln\frac{\exp\left(-\rho\left|y_F(\varsigma)-G_{\varsigma,\tau}h_F(\varsigma)\right|^2\right)}{\sum_{\gamma\neq\tau}\exp\left(-\rho\left|y_F(\varsigma)-G_{\varsigma,\gamma}h_F(\varsigma)\right|^2\right)}. \quad (20)$$

From (20), it can be found that comparing the LLR values for a given ς is equivalent to comparing the square Euclidean distances $|y_F(\varsigma)-G_{\varsigma,\tau}h_F(\varsigma)|^2$, $\tau=1,\ldots,n$, where the latter dispenses with any knowledge of the SNR. Since we have to search among $M(n-\gamma+1)$ constellation points only for the determination of the mode carried on the subcarrier q_γ, the computational complexity of the second step can be reduced to an order $\sim O(Mn^2/2+Mn/2)$ per bit block by resorting to the square Euclidean distance comparison.

3) Complexity Comparison: We take MM-OFDM-IM as a representative for comparison with classical OFDM in terms of the detection complexity. Table III lists the average number of metric calculations per subcarrier resulting by the brute-force ML, low-complexity ML, and subcarrier-wise detectors of the MM-OFDM-IM system, and the brute-force ML detector of the classical OFDM system, which are calculated as $M^n(n-1)!$, $Mn+2^{n-1}$, $Mn/2+M/2$, and M', respectively. To equate the SEs for both systems, we assume that the classical OFDM system employs M'-PSK/QAM with M' being obtained from interpolation. As disclosed by Table III, the brute-force ML detector of the MM-OFDM-IM system exhibits the highest detection complexity, which becomes intolerable with the increasing values of M or n. On the other hand, the proposed Viterbi-like algorithm can significantly reduce the total number of metric calculations. However, for large values of n, its detection complexity also overwhelms that of the brute-force ML detector of the classical OFDM system, and furthermore, a very large storage is required for its practical implementation. Finally, it is clear from Table III that the proposed subcarrier-wise detector of the MM-OFDM-IM system has a comparable detection complexity to the brute-force ML detector of the classical OFDM system. Actually, from (4), it is expected that

for large values of n, $M' \approx Mn/e$ and the increased number of metric calculations by employing the subcarrier-wise detector is only about $Mn/2+M/2-Mn/e$. In conclusion, we observe that MM-OFDM-IM provides an interesting trade-off between detection complexity and error performance compared to classical OFDM.

B. BER Upper Bound Analysis

In this subsection, we derive a tight upper bound for the BER of MM-OFDM-IM systems assuming the optimal ML detection. The analysis for the MM-OFDM-IM-IQ system can be conducted in a similar manner, and thus, is omitted for brevity.

From (5), the conditional pairwise error probability (PEP), which is defined as the probability of transmitting $\mathbf{X}$ and deciding on $\hat{\mathbf{X}}$ conditioned on $\mathbf{h}_F$, is given by

$$\Pr\left(\mathbf{X} \to \hat{\mathbf{X}} \middle| \mathbf{h}_F\right) = Q\left(\sqrt{\frac{\rho}{2}\left\|\left(\mathbf{X}-\hat{\mathbf{X}}\right)\mathbf{h}_F\right\|^2}\right). \quad (21)$$

Then, by resorting to the identity $Q(x) \approx 1/12 \cdot e^{-x^2/2} + 1/4 \cdot e^{-2x^2/3}$, the unconditioned PEP can be readily derived from (21) as [8]

$$\begin{aligned}\Pr\left(\mathbf{X} \to \hat{\mathbf{X}}\right) &= E_{\mathbf{h}_F}\left\{\Pr\left(\mathbf{X} \to \hat{\mathbf{X}} \middle| \mathbf{h}_F\right)\right\} \\ &= \frac{1/12}{\det\left(\mathbf{I}_n + (\rho/2)\mathbf{K}\mathbf{A}\right)} + \frac{1/4}{\det\left(\mathbf{I}_n + (2\rho/3)\mathbf{K}\mathbf{A}\right)}\end{aligned} \quad (22)$$

where $\mathbf{A} = (\mathbf{X}-\hat{\mathbf{X}})^H(\mathbf{X}-\hat{\mathbf{X}})$ and $\mathbf{K} = E_{\mathbf{h}_F}\{\mathbf{h}_F^H\mathbf{h}_F\}$ is the covariance matrix of $\mathbf{h}_F$. Finally, according to the union bounding technique, the BER of MM-OFDM-IM systems can be upper bounded by

$$P_e \le \frac{1}{p2^p}\sum_{\mathbf{X},\hat{\mathbf{X}}} \Pr\left(\mathbf{X} \to \hat{\mathbf{X}}\right) e\left(\mathbf{X}, \hat{\mathbf{X}}\right) \quad (23)$$

where $\Pr(\mathbf{X} \to \hat{\mathbf{X}})$ is given by (22) and $e(\mathbf{X}, \hat{\mathbf{X}})$ represents the number of bits in error for the corresponding pairwise error event. Due to the interleaving and de-interleaving operations, all subcarriers within a subcarrier group are separated with a certain frequency spacing that is usually larger than the coherence bandwidth of a practical channel, which implies $\mathbf{K} \approx \mathbf{I}_n$ [21]. Noting this property, we can approximate the upper bound in (23) as (24), shown at the bottom of this page, where $\hat{x}(\gamma)$ is the γ-th diagonal element of $\hat{\mathbf{X}}$ with $\gamma = 1, \ldots, n$.

To gain more insights, let us focus on the high SNR region, where $\rho \to +\infty$. As the probability of mistaking a symbol for some other than its nearest neighbor is considerably low for this case, (24) can be simplified according to the neighborhood approximation as

$$\begin{aligned}P_e &\le \frac{13}{24p2^p} \cdot \frac{\varepsilon(M)\,2^p n}{d_{intra}^2} \cdot \rho^{-1} + o(\rho^{-1}) \\ &= \frac{13/24}{\digamma_{\text{MM-OFDM-IM}}(M,n)} \cdot \frac{\varepsilon(M)}{d_{intra}^2} \cdot \rho^{-1} + o(\rho^{-1})\end{aligned} \quad (25)$$

where d_{intra} denotes the MIAD, $\varepsilon(M)$ represents the number of nearest neighbors that depends on the order as well as type of the modulation, and the Gray encoding for the M-ary signal constellation is assumed. The higher order term $o(\rho^{-1})$ in (25) can be shown to be a function of the MIAD and MIRD, which becomes negligible for extremely large ρ. As revealed in (25), to improve the asymptotic BER performance of MM-OFDM-IM systems, we should maximize the MIAD and MIRD, which has been pursued in this paper, and involve as more subcarriers as possible for multiple-mode transmission. However, the latter must be carefully balanced since the performance gain may be very small, as will be validated in Section VI, and comes at a cost of increased system complexity.

VI. Simulation Results and Comparisons

In this section, we perform computer simulations to examine the performance of MM-OFDM-IM(-IQ) systems, where Rayleigh fading channel and perfect channel estimation are assumed. The classical OFDM, OFDM-IM [8], DM-OFDM [34], and OFDM-I/Q-IM [17] schemes are chosen as reference in comparisons. For brevity, we will refer to "OFDM-IM (n, k), M-PSK(QAM)" as the OFDM-IM scheme with k out of n subcarriers are active and transmitting M-ary PSK (or QAM) symbols, "DM-OFDM (n, k), M-PSK(QAM)" as the DM-OFDM scheme with k out of n subcarriers employing the primary M-ary PSK (or QAM) constellation, "MM-OFDM-IM (M, n), PSK(QAM)" as the MM-OFDM-IM scheme with n subcarriers employing n different M-ary signal constellations under the PSK (or QAM) constraint, and "MM-OFDM-IM-IQ (M, n), PAM" as the MM-OFDM-IM-IQ scheme with both I- and Q- branches of n subcarriers employing n different M-ary signal constellations under the PAM constraint. It is worth noting that due to the same multiple-mode transmission nature, our study of the optimal modes for the MM-OFDM-IM scheme is extendable to the DM-OFDM scheme, which is not performed in [34].[4] Therefore, for fair comparison, we assume that the primary and secondary constellations employed by the DM-OFDM scheme follow our design guideline.

[4]We note that the MM-OFDM-IM scheme is not a straightforward generation of the DM-OFDM scheme. To carry two different modes, the MM-OFDM-IM scheme will require only two subcarriers, while the DM-OFDM scheme will use more than two.

$$\frac{1}{12p2^p}\sum_{\mathbf{X},\hat{\mathbf{X}}}\left[\prod_{\gamma=1}^{n}\left(1+\frac{\rho}{2}\left|x(\gamma)-\hat{x}(\gamma)\right|^2\right)^{-1} + 3\prod_{\gamma=1}^{n}\left(1+\frac{2\rho}{3}\left|x(\gamma)-\hat{x}(\gamma)\right|^2\right)^{-1}\right] e\left(\mathbf{X}, \hat{\mathbf{X}}\right) \quad (24)$$

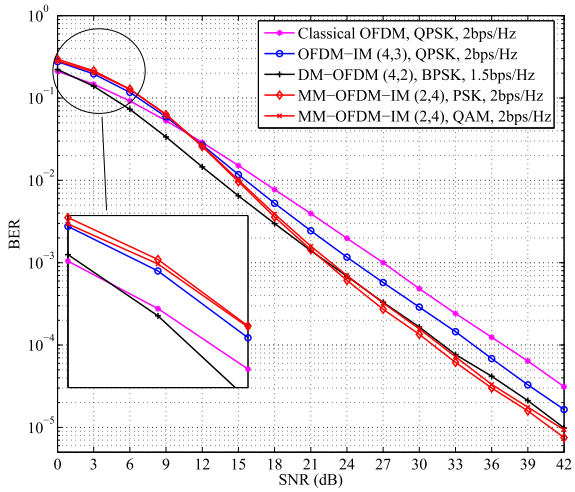

Fig. 7. Performance comparison between classical OFDM with QPSK, "OFDM-IM (4,3), QPSK", "DM-OFDM (4,2), BPSK", and "MM-OFDM-IM (2,4), PSK/QAM".

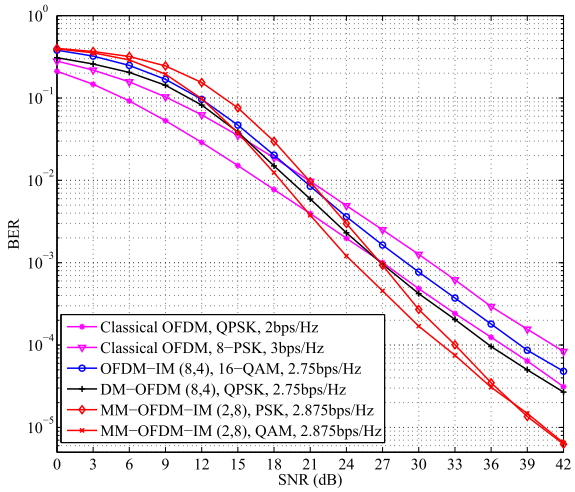

Fig. 8. Performance comparison between classical OFDM with QPSK/8-PSK, "OFDM-IM (8,4), 16-QAM"', "DM-OFDM (8,4), QPSK", and "MM-OFDM-IM (2,8), PSK/QAM".

A. Uncoded BER Performance

In this subsection, we make comparisons between MM-OFDM-IM(-IQ) and state-of-the-art schemes in terms of uncoded BER assuming the optimal ML detection for all schemes.

Fig. 7 shows the BER performance curves of classical OFDM with QPSK, "OFDM-IM (4,3), QPSK", "DM-OFDM (4,2), BPSK", and "MM-OFDM-IM (2,4), PSK/QAM", where all schemes achieve an SE of 2bps/Hz except "DM-OFDM (4,2), BPSK"' that has an SE of 1.5bps/Hz. As seen from Fig. 7, OFDM-IM outperforms classical OFDM in a reasonable SNR range. This can be understood since OFDM-IM provides a power saving with a factor of 25% due to the inactive subcarriers and one fourth of the IM bits have two-diversity-order protection, which corresponds to an SNR gain of $20\log_{10}(4/3) \approx 2.5$dB at high SNR. On the other hand, since DM-OFDM has an additional modulation gain of 3dB from QPSK to BPSK in spite of a loss in power gain, it still achieves SNR gains of about 2dB over OFDM-IM and 5dB over classical OFDM. Obviously, "MM-OFDM-IM (2,4), PSK' performs the best among all schemes in the SNR range of interest, achieving SNR gains of about 6dB over classical OFDM, which can be explained from Section V.B, and about 1dB over DM-OFDM, which can be accounted for the larger proportion of the IM bits despite having a higher SE. The relative performance between "MM-OFDM-IM (2,4), QAM" and "MM-OFDM-IM (2,4), PSK can be explained by their MIAD and MIRD. Since $d^{\text{PSK}}_{intra}(2) = 2 > d^{\text{QAM}}_{intra}(2,4) = 1.8257$, "MM-OFDM-IM (2,4), PSK" is superior to "MM-OFDM-IM (2,4), QAM" at high SNR. The intersection of the BER curves of both schemes at very low SNR below 6dB can be explained by the fact that $d^{\text{PSK}}_{inter}(2,4) = 0.7654 < d^{\text{QAM}}_{inter}(2,4) = 0.8165$ and the gap is much smaller than that between the MIADs.

Fig. 8 depicts the comparison results between classical OFDM with QPSK/8-PSK, "OFDM-IM (8,4), 16-QAM", "DM-OFDM (8,4), QPSK, and "MM-OFDM-IM (2,8), PSK/QAM" at an SE level of 2.875bps/Hz. Though it is not shown in the figure, the BER curve of classical OFDM at 2.875bps/Hz can be envisioned to be lying between those at 2bps/Hz and 3bps/Hz. As seen from Fig. 8, MM-OFDM-IM under either PSK or QAM constraint achieves SNR gains of about 6dB over classical OFDM with QPSK, about 7dB over OFDM-IM, and about 5dB over DM-OFDM at high SNR despite having a higher SE. Similarly, due to its larger MIAD and smaller MIRD, "MM-OFDM-IM (2,8), PSK" outperforms "MM-OFDM-IM (2,8), QAM" in the very high SNR region, whereas the situation is the opposite in the low-to-medium SNR region. The reason why the intersection lies at a higher SNR value than that in Fig. 7 can be attributed to the larger gap between the MIRDs, which are $d^{\text{PSK}}_{inter}(2,8) = 0.3902$ and $d^{\text{QAM}}_{inter}(2,8) = 0.6325$. Comparing Figs. 7 and 8, we can observe an interesting phenomenon that at very high SNR beyond 40dB, "MM-OFDM-IM (2,8), PSK" is even superior to "MM-OFDM-IM (2,4), PSK", although the former has a higher SE and a smaller MIRD than the latter. A mathematical explanation for this phenomenon has been given in (24) and the underlying reason is that the proportion of the IM bits in "MM-OFDM-IM (2,8), PSK" is larger than that in "MM-OFDM-IM (2,4), PSK", which alleviates the impact of the ordinary modulation bits on the BER more.

Fig. 9 presents the comparison results between classical OFDM with 32-QAM, "OFDM-IM (4,3), 64-QAM", "DM-OFDM (4,2), 16-PSK", and "MM-OFDM-IM (16,4), PSK/QAM", where all schemes achieve an SE of 5bps/Hz except "DM-OFDM (4,2), 16-PSK" that has an SE of 4.5bps/Hz. Similar to Figs. 7 and 8, MM-OFDM-IM performs considerably better than all other reference schemes. However, differently, the performance of "MM-OFDM-IM (16,4), QAM" overwhelms that of "MM-OFDM-IM (16,4), PSK" in the entire SNR region, since $d^{\text{QAM}}_{intra}(16,4) = 0.6172 > d^{\text{PSK}}_{intra}(16) = 0.3902$, $d^{\text{QAM}}_{inter}(16,4) = 0.3086 > d^{\text{PSK}}_{inter}(16,4) = 0.0981$. We conclude that MM-OFDM-IM scheme can overcome the main limitations of OFDM-IM

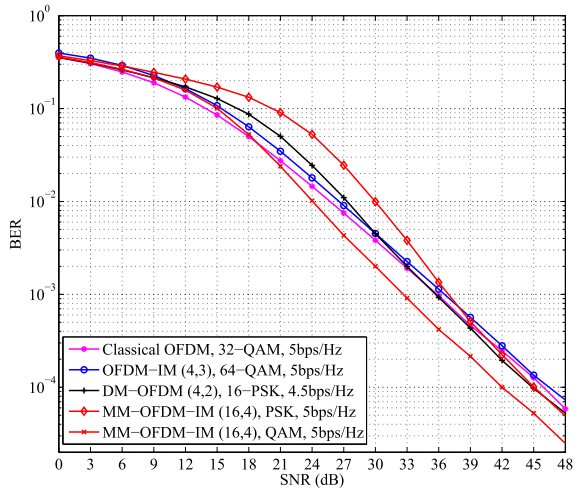

Fig. 9. Performance comparison between classical OFDM with 32-QAM, "OFDM-IM (4,3), 64-QAM", "DM-OFDM (4,2), 16-PSK", and "MM-OFDM-IM (16,4), PSK/QAM".

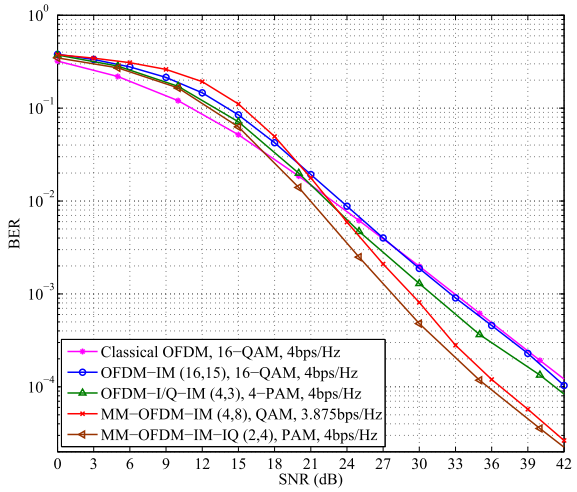

Fig. 10. Performance comparison between classical OFDM with 16-QAM, "OFDM-IM (16,15), 16-QAM", "OFDM-I/Q-IM (4,3), 4-PAM", and "MM-OFDM-IM-IQ (2,4), PAM".

and DM-OFDM schemes by providing an improved BER performance over classical OFDM even in higher SEs.

Finally, Fig. 10 illustrates the comparison results between classical OFDM with 16-QAM, "OFDM-IM (16,15), 16-QAM", "OFDM-I/Q-IM (4,3), 4-PAM, "MM-OFDM-IM (4,8), QAM", and "MM-OFDM-IM-IQ (2,4), PAM", where all schemes achieve an SE of 4bps/Hz except "MM-OFDM-IM (4,8), QAM" that has an SE of 3.875bps/Hz. The results verify the analysis given in [17], which proves that OFDM-I/Q-IM achieves SNR gains of about 2.5dB and 0.5dB over classical OFDM and OFDM-IM, respectively. However, when compared with MM-OFDM-IM-IQ, OFDM-I/Q-IM even has a BER deficit about 4dB. This can be explained by the fact that the modulation order employed by each subcarrier in MM-OFDM-IM-IQ is lower than that in OFDM-I/Q-IM while the proportion of the IM bits in MM-OFDM-IM, which is $1/2$, is higher than that in OFDM-I/Q-IM, which is $1/3$.

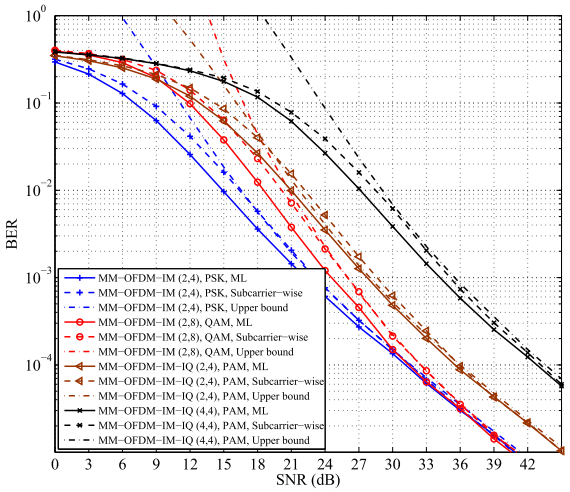

Fig. 11. Performance of the subcarrier-wise detectors of "MM-OFDM-IM (2,4), PSK", "MM-OFDM-IM (2,8), QAM", "MM-OFDM-IM-IQ (2,4), PAM", and "MM-OFDM-IM-IQ (4,4), PAM" and comparisons with BER upper bounds.

The same reason explains its superior performance over MM-OFDM-IM, despite MM-OFDM-IM-IQ has a higher SE. However, as revealed in Section IV.A, this advantage comes at a price of nearly double computational complexity.

B. Sub-Optimal Detection, Theoretical, and Achievable Rate Performance

In this subsection, we first evaluate the performance of the proposed subcarrier-wise detector and the derived theoretical upper bound for MM-OFDM-IM(-IQ) systems, and then compare the achievable rate of MM-OFDM-IM(-IQ) systems with those of state-of-the-art systems.

Fig. 11 gives the comparison results between the uncoded BER performance of the subcarrier-wise detectors and the optimal ML detectors for "MM-OFDM-IM (2,4), PSK", "MM-OFDM-IM (2,8), QAM", "MM-OFDM-IM-IQ (2,4), PAM", and "MM-OFDM-IM-IQ (4,4), PAM", where the derived theoretical BER upper bounds of those systems calculated by (24) are also shown with dash-dot curves. Due to the inherent problem of error propagation, the subcarrier-wise detector performs worse than the optimal ML detector at low-to-medium SNR region. Fortunately, as seen from Fig. 11, the performance loss is confined within 1.5dB. Specially, in the high SNR region, where the detection on each subcarrier becomes reliable and the error propagation is less likely to happen, the subcarrier-wise detector results in near-optimal performance. However, as revealed in Table III, its computational complexity is considerably lower than that of the ML detector. Therefore, for the scenarios in which the computational complexity must be carefully considered and the performance loss is sustainable, the subcarrier-wise detector can be the preferable option. On the other hand, it is clear from Fig. 11 that the proposed BER upper bounds provide accurate results for high SNR values.

Figs. 12 and 13 display the achievable rates of "MM-OFDM-IM (2,4), PSK", "MM-OFDM-IM (2,4), QAM", "MM-OFDM-IM (16,4), PSK", "MM-OFDM-IM (16,4),

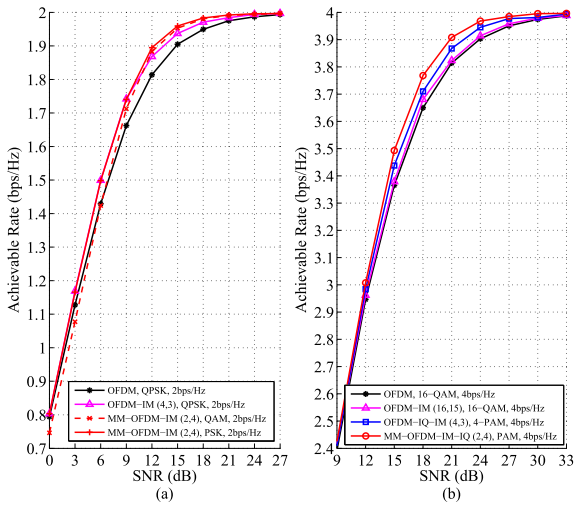

Fig. 12. Comparison between the achievable rates of "MM-OFDM-IM (2,4), PSK", "MM-OFDM-IM (2,4), QAM", "MM-OFDM-IM-IQ (2,4), PAM", and state-of-the-art systems at SEs of (a) 2bps/Hz and (b) 4bps/Hz.

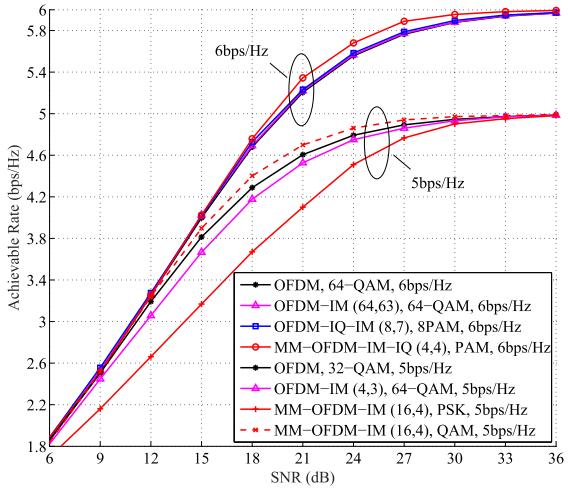

Fig. 13. Comparison between the achievable rates of "MM-OFDM-IM (16,4), PSK", "MM-OFDM-IM (16,4), QAM", "MM-OFDM-IM-IQ (4,4), PAM", and state-of-the-art systems at SEs of 5bps/Hz and 6bps/Hz.

QAM", "MM-OFDM-IM-IQ (2,4), PAM", and "MM-OFDM-IM-IQ (4,4), PAM", calculated in analogy with [21]. For comparison, the classical OFDM, OFDM-IM, and OFDM-I/Q-IM systems having the same SEs as those of MM-OFDM-IM(-IQ) systems are considered. As seen from Figs. 12 and 13, the achievable rates of all systems saturate at their corresponding transmitted information rates, namely SEs, at very high SNR due to the use of a finite alphabet input. Moreover, in consistence with the observation in uncoded scenarios, MM-OFDM-IM(-IQ) also outperforms its counterparts in terms of achievable rate for a large SNR range of interest, and its advantages over classical OFDM scheme are still prominent at high SEs.

VII. Conclusion and Remark

In this paper, we have proposed a multiple-mode transmission scheme called MM-OFDM-IM(-IQ) based on the OFDM framework. Unlike classical OFDM and OFDM-IM schemes, MM-OFDM-IM(-IQ) allows multiple subcarriers to transmit multiple different modes and utilizes the full permutation of these modes to convey additional information bits. A design guideline for the optimal mode selection has been presented, based on which the mode-selection strategy under the PSK/QAM/PAM constraint is designed. The optimal ML detector has been also proposed, which can be implemented via a Viterbi-like algorithm with reduced complexity. To further reduce the detection complexity, we have proposed an efficient subcarrier-wise detector, which shows near optimal performance. Finally, performance analyses and computer simulations have been conducted, showing that the MM-OFDM-IM(-IQ) scheme significantly outperforms the classical OFDM and existing OFDM-IM related schemes even in higher SEs.

We remark that in the presence of CFO or Doppler effects, strong ICI would arise in MM-OFDM-IM(-IQ) systems as in classical OFDM and DM-OFDM systems, since all subcarriers are filled with non-zero elements. The performance analysis and ICI mitigation for this case will be considered as our future work.

References

[1] M. Wen, X. Cheng, and L. Yang, *Index Modulation for 5G Wireless Communications* (Wireless Networks). Berlin, Germany: Springer, 2017.

[2] E. Başar, "Index modulation techniques for 5G wireless networks," *IEEE Commun. Mag.*, vol. 54, no. 7, pp. 168–175, Jul. 2016.

[3] R. Y. Mesleh, H. Haas, S. Sinanovic, C. W. Ahn, and S. Yun, "Spatial modulation," *IEEE Trans. Veh. Technol.*, vol. 57, no. 4, pp. 2228–2241, Jul. 2008.

[4] M. Di Renzo, H. Haas, A. Ghrayeb, S. Sugiura, and L. Hanzo, "Spatial modulation for generalized MIMO: Challenges, opportunities, and implementation," *Proc. IEEE*, vol. 102, no. 1, pp. 56–103, Jan. 2014.

[5] P. Yang, M. Di Renzo, Y. Xiao, S. Li, and L. Hanzo, "Design guidelines for spatial modulation," *IEEE Commun. Surveys Tuts.*, vol. 17, no. 1, pp. 6–26, 1st Quart., 2015.

[6] R. Abu-alhiga and H. Haas, "Subcarrier-index modulation OFDM," in *Proc. IEEE 20th Int. Symp. Pers., Indoor Mobile Radio Commun. (PIMRC)*, Tokyo, Japan, Sep. 2009, pp. 177–181.

[7] D. Tsonev, S. Sinanovic, and H. Haas, "Enhanced subcarrier index modulation (SIM) OFDM," in *Proc. IEEE GLOBECOM Workshops (GC Wkshps)*, Houston, TX, USA, Dec. 2011, pp. 728–732.

[8] E. Başar, U. Aygölü, E. Panayirci, and H. V. Poor, "Orthogonal frequency division multiplexing with index modulation," *IEEE Trans. Signal Process.*, vol. 61, no. 22, pp. 5536–5549, Nov. 2013.

[9] P. K. Frenger and N. A. B. Svensson, "Parallel combinatory OFDM signaling," *IEEE Trans. Commun.*, vol. 47, no. 4, pp. 558–567, Apr. 1999.

[10] G. Kaddoum, M. F. A. Ahmed, and Y. Nijsure, "Code index modulation: A high data rate and energy efficient communication system," *IEEE Commun. Lett.*, vol. 19, no. 2, pp. 175–178, Feb. 2015.

[11] G. Kaddoum and E. Soujeri, "On the comparison between code-index modulation and spatial modulation techniques," in *Proc. IEEE Int. Conf. Inf. Commun. Technol. Res. (ICTRC)*, Abu Dhabi, United Arab Emirates, May 2015, pp. 24–27.

[12] G. Kaddoum, Y. Nijsure, and H. Tran, "Generalized code index modulation technique for high-data-rate communication systems," *IEEE Trans. Veh. Technol.*, vol. 65, no. 9, pp. 7000–7009, Sep. 2016.

[13] Y. Bian, X. Cheng, M. Wen, L. Yang, H. V. Poor, and B. Jiao, "Differential spatial modulation," *IEEE Trans. Veh. Technol.*, vol. 64, no. 7, pp. 3262–3268, Jul. 2015.

[14] R. Padovani and J. Wolf, "Coded phase/frequency modulation," *IEEE Trans. Commun.*, vol. COM-34, no. 5, pp. 446–453, May 1986.

[15] S. Hong, M. Sagong, C. Lim, S. Cho, K. Cheun, and K. Yang, "Frequency and quadrature-amplitude modulation for downlink cellular OFDMA networks," *IEEE J. Sel. Areas Commun.*, vol. 32, no. 6, pp. 1256–1267, Jun. 2014.

[16] M. Wen, Y. Zhang, J. Li, E. Başar, and F. Chen, "Equiprobable subcarrier activation method for OFDM with index modulation," *IEEE Commun. Lett.*, vol. 20, no. 12, pp. 2386–2389, Dec. 2016.
[17] B. Zheng, F. Chen, M. Wen, F. Ji, H. Yu, and Y. Liu, "Low-complexity ML detector and performance analysis for OFDM with in-phase/quadrature index modulation," *IEEE Commun. Lett.*, vol. 19, no. 11, pp. 1893–1896, Nov. 2015.
[18] Y. Xiao, S. Wang, L. Dan, X. Lei, P. Yang, and W. Xiang, "OFDM with interleaved subcarrier-index modulation," *IEEE Commun. Lett.*, vol. 18, no. 8, pp. 1447–1450, Aug. 2014.
[19] X. Cheng, M. Wen, L. Yang, and Y. Li, "Index modulated OFDM with interleaved grouping for V2X communications," in *Proc. IEEE 17th Int. Conf. Intell. Trans. Syst. (ITSC)*, Oct. 2014, pp. 1097–1104.
[20] Y. Ko, "A tight upper bound on bit error rate of joint OFDM and multi-carrier index keying," *IEEE Commun. Lett.*, vol. 18, no. 10, pp. 1763–1766, Oct. 2014.
[21] M. Wen, X. Cheng, M. Ma, B. Jiao, and H. V. Poor, "On the achievable rate of OFDM with index modulation," *IEEE Trans. Signal Process.*, vol. 64, no. 8, pp. 1919–1932, Apr. 2016.
[22] M. Wen, X. Cheng, and L. Yang, "Optimizing the energy efficiency of OFDM with index modulation," in *Proc. IEEE Int. Conf. Commun. Syst. (ICCS)*, Nov. 2014, pp. 31–35.
[23] Q. Ma, Y. Xiao, L. Dan, P. Yang, L. Peng, and S. Li, "Subcarrier allocation for OFDM with index modulation," *IEEE Commun. Lett.*, vol. 20, no. 7, pp. 1469–1472, Jul. 2016.
[24] A. I. Siddiq, "Low complexity OFDM-IM detector by encoding all possible subcarrier activation patterns," *IEEE Commun. Lett.*, vol. 20, no. 3, pp. 446–449, Mar. 2016.
[25] E. Başar, "OFDM with index modulation using coordinate interleaving," *IEEE Wireless Commun. Lett.*, vol. 4, no. 4, pp. 381–384, Aug. 2015.
[26] Q. Ma, P. Yang, Y. Xiao, H. Bai, and S. Li, "Error probability analysis of OFDM-IM with carrier frequency offset," *IEEE Commun. Lett.*, vol. 20, no. 12, pp. 2434–2437, Dec. 2016.
[27] M. Wen, X. Cheng, L. Yang, Y. Li, X. Cheng, and F. Ji, "Index modulated OFDM for underwater acoustic communications," *IEEE Commun. Mag.*, vol. 54, no. 5, pp. 132–137, May 2016.
[28] N. Ishikawa, S. Sugiura, and L. Hanzo, "Subcarrier-index modulation aided OFDM—Will it work?" *IEEE Access*, vol. 4, pp. 2580–2593, Jun. 2016.
[29] E. Başar, "Multiple-input multiple-output OFDM with index modulation," *IEEE Signal Process. Lett.*, vol. 22, no. 12, pp. 2259–2263, Dec. 2015.
[30] E. Başar, "On multiple-input multiple-output OFDM with index modulation for next generation wireless networks," *IEEE Trans. Signal Process.*, vol. 64, no. 15, pp. 3868–3878, Aug. 2016.
[31] B. Zheng, M. Wen, E. Başar, and F. Chen, "Multiple-input multiple-output OFDM with index modulation: Low-complexity detector design," *IEEE Trans. Signal Process.*, vol. 65, no. 11, pp. 2758–2772, Jun. 2017.
[32] H. Zhang, L.-L. Yang, and L. Hanzo, "Compressed sensing improves the performance of subcarrier index-modulation-assisted OFDM," *IEEE Access*, vol. 4, pp. 7859–7873, Oct. 2016.
[33] R. Fan, Y. J. Yu, and Y. L. Guan, "Generalization of orthogonal frequency division multiplexing with index modulation," *IEEE Trans. Wireless Commun.*, vol. 14, no. 10, pp. 5350–5359, Oct. 2015.
[34] T. Mao, Z. Wang, Q. Wang, S. Chen, and L. Hanzo, "Dual-mode index modulation aided OFDM," *IEEE Access*, vol. 5, pp. 50–60, 2017.
[35] G. Foschini, R. Gitlin, and S. Weinstein, "Optimization of two-dimensional signal constellations in the presence of Gaussian noise," *IEEE Trans. Commun.*, vol. 22, no. 1, pp. 28–38, Jan. 1974.
[36] G. Ungerboeck, "Channel coding with multilevel/phase signals," *IEEE Trans. Inf. Theory*, vol. IT-28, no. 1, pp. 55–67, Jan. 1982.
[37] M. Wen, X. Cheng, Y. Bian, and H. V. Poor, "A low-complexity near-ML differential spatial modulation detector," *IEEE Signal Process. Lett.*, vol. 22, no. 11, pp. 1834–1838, Nov. 2015.
[38] A. J. Viterbi, "Error bounds for convolutional codes and an asymptotically optimum decoding algorithm," *IEEE Trans. Inf. Theory*, vol. IT-13, no. 2, pp. 260–269, Apr. 1967.

Miaowen Wen (M'14) received the B.S. degree from Beijing Jiaotong University, Beijing, China, in 2009, and the Ph.D. degree from Peking University, Beijing, in 2014. From 2012 to 2013, he was a Visiting Student Research Collaborator with Princeton University, Princeton, NJ, USA. Since 2014, he has been a faculty member of the South China University of Technology, Guangzhou, China. He has authored a book and over 60 papers in refereed journals and conference proceedings. His current research interests include index modulation and nonorthogonal multiple access techniques.

He received the Best Paper Award at the IEEE International Conference on Intelligent Transportation Systems Telecommunications in 2012, the IEEE International Conference on Intelligent Transportation Systems in 2014, and the IEEE International Conference on Computing, Networking and Communications in 2016. He received the Excellent Doctoral Dissertation Award from Peking University. He is serving as a Guest Editor for a Special Section at the IEEE ACCESS.

Ertugrul Basar (S'09–M'13–SM'16) received the B.S. degree (Hons.) from Istanbul University, Turkey, in 2007, and the M.S. and Ph.D. degrees from Istanbul Technical University, in 2009 and 2013, respectively. He spent the academic year 2011–2012 with the Department of Electrical Engineering, Princeton University, NJ, USA. He was an Assistant Professor with Istanbul Technical University from 2014 to 2017, where he is currently an Associate Professor of Electronics and Communication Engineering. His primary research interests include MIMO systems, index modulation, cooperative communications, OFDM, and visible light communications. He is an Inventor of two pending patents on index modulation schemes. He is also a Reviewer of various IEEE journals, and has served as a TPC member for several conferences. He was a recipient of the Istanbul Technical University Best Ph.D. Thesis Award in 2014 and has received four best paper awards, including one from the IEEE International Conference on Communications 2016. He currently serves as an Associate Editor of the IEEE COMMUNICATIONS LETTERS and the IEEE ACCESS.

Qiang Li received the B.S. degree from the Inner Mongolia University of Science and Technology, Baotou, China, in 2013, and the M.S. degree from the Nanjing University of Aeronautics and Astronautics, Nanjing, China, in 2016. He is currently pursuing the Ph.D. degree with the South China University of Technology, Guangzhou, China. His recent research interests include MIMO systems, index modulation, and OFDM.

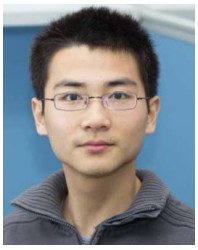

Beixiong Zheng received the B.S. degree from the South China University of Technology, Guangzhou, China, in 2013, where he is currently pursuing the Ph.D. degree. Since 2015, he has been a Visiting Student Research Collaborator with Columbia University, New York City, NY, USA. His recent research interests include spatial modulation, nonorthogonal multiple access, and pilot multiplexing techniques. He received the Best Paper Award at the IEEE International Conference on Computing, Networking and Communications in 2016.

Meng Zhang was born in Shandong, China. He received the B.S. degree in electronics engineering from the School of Electronics Engineering and Computer Science, Peking University, China, in 2014. He is currently pursuing the M.S. degree in signal and information processing with the Modern Communications Research Institute, Peking University. His current research interests include spatial modulation, OFDM, and wireless powered communications. He was a recipient of the IEEE Microsoft Student Application Paper Grants.